Title

PARTICLE YIELDS AT SLAC AND THE PHOTON-NUCLEUS INTERACTION IN THE 5-18 GeV REGION

Authors

Flatte, Stanley M.
Murray, Joseph J.
KLein, Paul R.
et al.

Publication Date

1967-07-21

UCRL-17687

cy. 2

University of California

Ernest O. Lawrence Radiation Laboratory

PARTICLE YIELDS AT SLAC AND
THE PHOTON-NUCLEUS INTERACTION IN THE 5-18 GeV REGION

Stanley M. Flatté, Joseph J. Murray, Paul R. Klein,
Lawrence H. Johnston, and Stanley G. Wojcicki

July 21, 1967

Berkeley, California

DISCLAIMER

Submitted to The Physical Review
Also to be submitted to the 1967
International Symposium on Electron
and Photon Interactions at High
Energies, Sept. 5-9, 1967, SLAC

UCRL-17687
Preprint

UNIVERSITY OF CALIFORNIA

Lawrence Radiation Laboratory
Berkeley, California

AEC Contract No. W-7405-eng-48

PARTICLE YIELDS AT SLAC AND THE PHOTON-NUCLEUS INTERACTION IN THE 5-18 GeV REGION

Stanley M. Flatté, Joseph J. Murray, Paul R. Klein,
Lawrence H. Johnston, and Stanley G. Wojcicki

July 21, 1967

PARTICLE YIELDS AT SLAC AND THE PHOTON-NUCLEUS INTERACTION IN THE 5-18 GeV REGION*

Stanley M. Flatté and Joseph J. Murray†

Lawrence Radiation Laboratory, University of California, Berkeley, California

Paul R. Klein

Department of Physics, Purdue University, West Lafayette, Indiana

Lawrence H. Johnston

Stanford Linear Accelerator Center, Stanford University, Stanford, California

and

Stanley G. Wojcicki

Department of Physics, Stanford University, Stanford, California

July 21, 1967

ABSTRACT

Yields of $\pi^{\pm}$, $K^{\pm}$, $p^{\pm}$, and $e^{\pm}$ at 2 and 3 deg from 16- and 18-GeV electrons on three different targets have been measured at the Stanford two-mile electron accelerator. The targets were: 0.3 radiation length (r.l.) of Be, 0.3 r.l. of Fe, and a combination consisting of 0.6 r.l. of Fe followed by 0.3 r.l. of Be. The yields are discussed in terms of the Drell mechanism (for $\pi^{\pm}$, $K^{\pm}$, $p^{\pm}$), ρ production ($\pi^{\pm}$), associated production from pions produced by photons (K^{+}), photodisintegration (p^{+}), and elastic scattering (e^{-}). The A dependences of the yields have been determined from the ratio of the Be- and the Fe-target yields.

I. INTRODUCTION

The new 20-GeV Stanford electron accelerator provides a unique opportunity for the study of the photon-nucleus interaction at energies much greater than previously available. Expectations that this new energy region would be interesting were greatly enhanced by Drell, who, in 1960, calculated the amplitudes for a particular set of photon-induced peripheral processes which produce strongly interacting particles.[1] At energies up to 6 GeV it has been found that these peripheral processes account for a large part, though not all, of pion production, and it was anticipated that at higher energies these processes would more completely dominate the cross section for forward angles.[2] As an added fillip, Drell's calculations were used to predict yields of secondary particles at SLAC that were large enough to be experimentally useful.[3] Later it was realized that another important mechanism, ρ production, contributes to the $\pi^{\pm}$ yields.[4]

While engaged in an experiment[5] to determine the usefulness of some secondary particle beams at SLAC, we have gathered data on secondary particle yields from targets exposed directly to the electron beam. This article differs in substance from Ref. 5 principally in the inclusion of data from an Fe target and an Fe-Be combination target (see Table I), and data on the time distribution of the secondary beams (see Sec. IV). Although the data are by no means complete, we feel they constitute enough information to allow some useful, though preliminary, conclusions. Basically, the experimental results indicate that, with two notable exceptions, the yields of strongly interacting particles roughly agree with the predictions of the Drell mechanism plus ρ production (Drell + ρ).

The first exception is the K^+ yields, which are 1.6 to 3.7 times the K^- yields, where 1.3 is expected from the Drell mechanism. The most logical explanation for the excess K^+ is the process $\pi p \rightarrow K^+ \Lambda (\Sigma)$, taking place in the same nucleus where a photon has produced the π; however, no direct evidence of this process is given.[6] The second exception is the proton yields, which are 10 times the $\bar{p}$ yields. Here processes of photodisintegration (where a proton is "knocked out" of the nucleus) are invoked, again with no direct confirmation.[7]

Although the absolute magnitude of the yields does agree reasonably well with Drell + ρ, their momentum and angle dependences are not in quantitative agreement. The effects of final-state interactions will definitely modify the Drell + ρ predictions toward agreement; however, no method of quantitative calculation is known.

In Sec. V we discuss these theoretical questions in more detail, as well as covering the implications of the bremsstrahlung photon spectrum within the target, the A dependences of the yields, and the electron yields.

We have also measured the radio-frequency structure of the secondary beam, which results from the "bunching" of the accelerator beam. The results are presented, along with the yields, in Sec. IV.

II. EXPERIMENTAL APPARATUS AND PROCEDURE

A. Primary and Secondary Beams

A beam of electron pulses was provided by the Stanford 20-GeV linear accelerator. The normal pulse rate during the experiment was 180 pulses per second, with each pulse containing about 10^{10} electrons and lasting 1.5 μsec. The energy of the electrons was 18 GeV (a few runs were at 16 GeV), with an energy spread of < 1%. The beam "spot size" at our target was about 0.3 cm vertically and 0.5 cm horizontally, the larger horizontal dimension arising from some momentum dispersion due to the guiding magnets ahead of our target.

We used three different targets in the experiment. Our basic target was a 10-cm length of beryllium, (≈0.3 radiation length). In order to determine the dependence of the yields on the atomic weight of the target nuclei, we used an iron target with a length of 0.54 cm (≈0.3 radiation length, and made to correspond as closely as possible to the number of radiation lengths in 10 cm of Be). The purpose of our third target was more utilitarian: to determine the maximum yield obtainable from a 10-cm-long target. This third target was 10 cm of Be preceded by 0.95 cm (≈0.6 radiation length) of iron. The interpretation of the results from this target is given in Sec. V. B.

The primary-beam monitor system is described in another publication.[8] Briefly, a signal from the target (which was electrically insulated) provided a measure of the net charge leaving the target over any period of time. By comparing the absolute magnitude of the electron beam current, as measured by calibrated toroids, with the electrical signal from the target when all the beam was hitting the target, we

obtained an absolute calibration of the target signal. The results were that the Be, Fe, and Be-Fe-combination targets were 125%, 21%, and 292% efficient, respectively. An efficiency of 100% means that for each electron in the primary beam entering the target, two electrons leave the target (where one of these may of course be the primary electron). Since the calibrated toroids on which this measurement was based are accurate to ±5%, the uncertainty in the absolute normalization of the primary electron beam current is ±5%.

Figure 1(a) shows the beam layout. The quadrupole doublet focused particles of the desired momentum onto the counter array. The bending magnet provided momentum resolution at the counters. The three-foot-long lead collimators C1 and C2 defined the solid-angle acceptance in an easily calculable way. A continuous vacuum system covered the entire beam line.

The solid angle accepted by the system was 8.2 μsr and the momentum resolution was 0.90%.

B. Counter Array

Figure 1(b) shows the counter array, which was designed to detect and separate electrons, pions, kaons, protons, and muons. Here S_1 through S_5 were plastic scintillators, C_1 and C_2 were Čerenkov counters, and D_1 and D_2 were microwave-gated photomultipliers, referred to in the literature as DCFEM's.[9]

The spatial acceptance of the counter array was determined by S_2 and S_3 near the beam focus and S_1 which defined an angular aperture of ≈7 mr.

C. Electron and Muon Separation

Scintillator S_4 detected showers produced by electrons interacting in the preceding lead. The thickness of lead was experimentally adjusted to be near the shower maximum for each momentum studied, and the discriminator on S_4 was set to reject single particles and accept only electron showers. Figure 2 illustrates the development of an electron shower by showing the counts obtained in S_4 (in coincidence with $S_1S_2S_3$) for various discriminator settings and various thicknesses of lead. The voltage of S_4 was set so that, with no lead, $S_1S_2S_3S_4$ did not count. The data was obtained with the 6-GeV/c secondary beam from the Be target, because at 6 GeV/c the Čerenkov counters (see next section) provided independent information about the fraction of electrons in the beam. The Čerenkov result was $44 \pm 2\%$ for the percentage of electrons in the beam, and we see that the curve with 7/8 in. of lead forms a plateau at 46%, consistent with the Čerenkov results. The plateau obtained at 6 GeV/c is not very impressive except in the context of the whole family of curves, because of a relatively small multiplicity at the shower maximum. As the momentum is increased the number of particles at the shower maximum increases, and the plateau improves. This is illustrated in Fig. 3. Hence we believe the S_4-Pb system counts electrons with an efficiency of 98% or better. By studying the particle beams with plus charges where there is small positron percentage, we have determined that pions can trigger the S_4-Pb system approximately 4% of the time, probably by π^0 production with subsequent showers from the γ-rays. Thus if we measure an electron percentage of 50%, it means that actually 48% of the beam was electrons. We have, therefore, a

system which can separate electrons (or positrons) from all other particles at momenta for which our Čerenkov counters are not effective for this purpose (i.e., above 6 GeV/c).

Scintillator S_5, together with iron absorbers placed in front of it, measured the μ percentage in the beam. The diameter of S_5 was calculated to catch more than 95% of the muons, at 12 GeV/c, and to catch other particles < 1% of the time, when five feet of iron was put in place. Figure 4 shows a measurement of $S_1S_2S_3C_1C_2S_5$ counts at 12 GeV/c as a function of the length of iron absorber. We see that muons form < 1% of the beam.

D. Čerenkov Counters

The Čerenkov counters are relatively simple in construction, and weigh less than twenty pounds each; two of them in coincidence are capable of a resolution comparable with that of the large counters of Kycia and Jenkins.[10] The Čerenkov counters consist of a 1-m-long steel pipe with a 1-in. i.d., cylindrical glass tube, aluminized on the inside, mounted in the pipe by means of aluminum spacers. The fittings on both ends of the counter provided 50-mil Al windows for the beam to pass through, and at one end a 45-deg mirror of glass aluminized on one side turned the Čerenkov light through 90 deg where it exited from the pipe through a quartz window. For the threshold counter we simply put the phototube against the quartz window. For the differential counter a quartz lens with 16-in. focal length was put against the quartz window and a 100-mil-wide, 1.5-in.-diameter annulus was mounted in the focal plane of the lens, with the phototube just behind the annulus. The Čerenkov angle prescribed by the differential counter was thus 2.7 deg.

The essential characteristic of the experiment which made it possible to use such simple counters was the small spatial extent (<3/4-in. diameter) of the beam at the counter array. The counter was further kept small by the aluminized glass tube which confined the Čerenkov light to a 1-in. aperture without destroying any of its useful characteristics. The small aperture also reduced the effects of chromatic aberration in the quartz lens.

Counter C_1 was filled with nitrogen gas at a pressure such that it would not count K's but only π-μ-e. Counter C_2 was filled with Freon 13 (a few times with N_2). To study the π-μ-e region we recorded the coincidence counts $S_1S_2S_3$ and $S_1S_2S_3C_2$ at various pressures in C_2. Above the π-μ-e region, where we needed additional rejection against fast particles in order to clearly see the K and p peaks, we recorded $S_1S_2S_3\bar{C}_1C_2$ as a function of pressure in C_2. The separating power of these two counters is illustrated in Fig. 5. From these figures, which are raw recorded data, we can read off directly the percentages of K, p, and, at the lower momenta, π and e in the beam.

The resolution of the differential counter, as measured by $\Delta\beta/\beta$, can be determined from the width of the peaks as a function of pressure. A width of 8 lb/in.^{2} corresponds to a $\Delta\beta/\beta = 4 \times 10^{-4}$. The noticeable flattop on the peaks indicates that we could have improved the resolution somewhat by narrowing the annulus. However, the $\Delta\beta/\beta = 4 \times 10^{-4}$ was adequate.

E. DCFEM

The counters labelled D1 and D2 in Fig. 1(b) are microwave-gated photomultipliers (DCFEM).[9] We have designed and built several of these photomultiplier tubes, and their characteristics are described fully in another publication.[11] However, in order to present the results here we need to briefly explain those DCFEM properties which were useful to us.

The linear accelerator uses electromagnetic fields with a frequency of 2856 Mc to accelerate the electrons. This introduces a bunch structure over the rf period; that is, the electrons emerge from the accelerator in tight bunches, 0.3 nsec apart, with widths small compared to their separation.[12] We wanted to investigate this structure in order to predict the efficacy of an rf deflector in providing separated secondary particle beams at SLAC. For these secondary beams we needed information about the width of the bunches and the relative numbers of particles during the part of the rf cycle off the bunch. Unfortunately no ordinary time-of-flight system in particle detection can probe to such small time intervals. However, the DCFEM can, as will be shown.

The DCFEM, schematically illustrated in Fig. 6, consists of two plane parallel plates with an rf electric field perpendicular to the plates, and a static magnetic field H parallel to the plates. A photo-sensitive, secondary emitter is laid down in a strip perpendicular to H on one of the plates. When a photon strikes one end of the strip, releasing secondary electrons, one of two things occurs: In the first, the photon arrives at a time in the rf cycle when its secondary electron will be accelerated away from the plate, in which case the electron executes a cycloid-like

orbit and strikes the plate with a large enough energy to release more secondary electrons which propagate down the strip, multiplying as they go, until they are collected on an insulated electrode to form a signal. In the second, the photon arrives at a time in the rf cycle when the secondary electron will be forced back into the plate with very little energy, causing the electron to be absorbed. In order for the cycloid-like orbits to propagate, the magnetic field and electric field must be in certain ratios. In this manner we have developed a phase-sensitive photomultiplier. That is, the DCFEM translates the time a photon arrives into a pulse height on the collector. Of course the actual dynamics are not so clean-cut as we have implied; in fact, the multiplier as we have built it has a pulse-height ratio between the "best" phase and the "worst" phase of four, and a pulse-height distribution similar to that shown in Fig. 7, which was derived by computer simulation of the dynamics and the secondary emission process.[11]

The DCFEM's were mounted on Čerenkov radiators, which supplied the photons from the charged particles whose time structure we wished to investigate. We used rf power which was phased with the linac power, and we could vary the phase of the DCFEM with respect to the linac (and hence with respect to the electron bunches). The experiment then consisted of choosing a particular type of particle with the Čerenkov counters (C_1 and C_2) and scintillators, and varying the phase of the DCFEM, with the output of the DCFEM put through a discriminator and into coincidence with the other counters. DCFEM results are given in Sec. IV.

III. SCATTERING AND INTERACTION CORRECTIONS

The raw data were taken in the following way: First we measured the ratio of the number of coincidence counts in $S_1S_2S_3$ to the total charge integrated by the beam monitor system in a given time interval. We call this ratio R_{Mon}; it represents the total yield (of all particles we measure) per primary beam electron. The percentage of a given particle in the beam is then obtained from graphs like those in Fig. 5. However, these raw numbers must be corrected for losses due to scattering and interaction in the material in the counter array. These losses of course mean that the R_{Mon} should be increased by some amount, but they also mean that the percentage of a certain particle measured at a certain pressure in C_2 must be corrected, because $e^{\pm}$ have no strong interactions, and thus are affected differently by the material than are π, K, and p.

Let us call R_{Norm} the corrected ratio of $S_1S_2S_3$ to monitor integral. We use a very simple correction equation

$$R_{Mon} = R_{Norm}\, e^{-\ell/\ell_i}\, e^{-(\theta/\sigma)^2} \qquad (1)$$

where ℓ is the length of material, ℓ_i is the interaction length of the material, θ is the rms angle of scattering for the material, and σ is an angle characteristic of the geometry of the counter array, which we determine empirically.

The material in the counter array which affects R_{Mon} includes S_1, S_2, windows and mirrors in C_1 and C_2, the vacuum pipe window, 2 meters of air space, 50 psia N_2 in C_1, and a variable amount of gas in

C_2. To find the effective ℓ/ℓ_i we must know ℓ_i, the interaction length in g/cm^2, for all the materials. To find the effective θ^2 we must know the radiation length in g/cm^2 for all the materials. Numerically equation (1) becomes

$$R_{Norm} = R_{Mon} \exp\left\{[0.063 + 4.2\times10^{-4} P_G] + \left(\frac{21}{p\sigma}\right)^2 [0.146 + 1.11\times10^{-3} P_G]\right\}, \quad (2)$$

where P_G is the pressure in psia of Freon in C_2, p is the momentum (in GeV/c) of the secondary beam, and σ is in mrad.

It is important to realize that Equations (1) and (2) are valid only for π, K, and p. For electrons the interaction correction must be removed. This introduces a modification to the formula, giving

$$R_{Norm} = R_{Mon}\, e^{(\theta/\sigma)^2} \left\{ f^e + (1 - f^e)\, e^{\ell/\ell_i} \right\}, \quad (3)$$

where f^e is the percentage of electrons in the beam. In the application of this formula we have used the observed percentage of electrons rather than the corrected one; this is a very good approximation and makes calculation easier.

The equation for calculating the corrected percentage of electrons is

$$f^e_{corr} = f^e_{obs} \left\{ f^e_{obs} + (1 - f^e_{obs})\, e^{\ell/\ell_i} \right\}^{-1}, \quad (4)$$

where ℓ/ℓ_i is evaluated for the pressure in C_2 at which the measurement of f^e_{obs} was made. The equation for calculating the corrected percentage of π, K, or p is

$$f_{corr} = f_{obs}\, e^{\ell/\ell_i} \left\{ f^e_{obs} + (1 - f^e_{obs})\, e^{\ell/\ell_i} \right\}^{-1} \qquad (5)$$

where ℓ/ℓ_i is evaluated at the pressure in C_2 corresponding to the peak for the particle in question. In these last two formulas we have again used f^e_{obs} where we should have used f^e_{corr}; the difference in the correction factor is negligible.

In order to determine σ we need only compare $R_{Mon} \times f^e_{obs}$ at two different pressures in C_2. Since $R_{Norm} \times f^e_{corr}$ stays the same by definition, we may solve for σ. Using data from a 2 deg production angle, 18-GeV incident electrons, and the Be target, we find for both the 4-GeV/c and 12-GeV/c secondary beams that $\sigma = 5.2$ mrad. The fact that the same value of σ is valid for the extremes of momenta, and that the value of σ is quite reasonable for the counter geometry, gives us confidence that the equation has physical meaning.

Once σ is determined we can check the coefficient of P_G in the first parenthesis of the exponential of Eq. (2) by comparing R_{Mon} at two different pressures in C_2. At both 4 GeV/c and 12 GeV/c this coefficient checks well with experimental values. Thus again we are given confidence that the equation is useful.

The total scattering plus interaction correction is typically 15%.

IV. EXPERIMENTAL RESULTS

A. DCFEM Results

1. rf Bunch Width

In order for one to determine the rf bunch width of the secondary beam, it would be ideal if the DCFEM were sensitive to a very narrow phase interval and insensitive elsewhere. As Fig. 7 shows, this is not the case; it is sensitive over about 180 deg of phase. However, the edge of the sensitive region is quite steep, and this property allows us to determine a reasonable upper limit for the bunch width. Figure 8 shows the detection efficiency of the DCFEM as a function of phase for 10-GeV/c electrons. Since the DCFEM output is put through a discriminator, to relate Fig. 8 with Fig. 7 one must know the discrimination level and the number of photons generated by a charged particle in the Čerenkov radiator. Note that the experimental measurements are 30 deg apart in phase; this distance corresponds to ≈ 0.03 nsec. The slope of the sharp edge of the efficiency function in Fig. 8 represents a folding of the actual DCFEM properties with the finite width of the secondary electron bunch. The derivative of this slope, also shown in Fig. 8, thus provides an upper limit to the secondary beam bunch width. The result is: The full-width at half-maximum of the secondary beam bunch is less than 20 deg of the rf cycle. We obtain a better limit of 10 deg from Fig. 9 (see next paragraph).

2. Off-Time Background

Even though the bulk of the secondary beam is bunched within a small fraction of the rf cycle, it is important to know how much beam is contained in the part of the cycle outside the bunch. Since rf separators

can be required to reject unwanted particles 1000 times more copious than the wanted particles, we need to measure the off-time background to a level of one-thousandth of the total beam. In order to accomplish this we put two DCFEM's in coincidence, each of which separately gave an apparent indication that the off-time background was less than 3% of the beam. Figure 9 shows the result. When the DCFEM sensitive region is centered on the main beam bunch, the efficiency is 40%. When the sensitive region covers one half-cycle centered between beam bunches, the efficiency is $< 0.025\%$. Hence the off-time background is less than 0.6×10^{-3} of the main beam. This result is for π^+ at 12 GeV/c, at a production angle of 2 deg, and with 18-GeV primary electrons. We also measured an off-time background for negative fast particles (77% e^- and 23% π^-) at 12 GeV/c from 18-GeV primary electrons and at a production angle of 3 deg. The background there was less than 2×10^{-3} of the main beam.

3. Time-of-Flight of π, K, and p

The secondary electrons, pions, kaons, and protons created in the target by the primary electrons have the same rf bunch structure as the primary electrons. However, as the secondaries leave the target they disperse in time due to their range of velocities. If we choose a definite momentum--12 GeV/c--and a definite flight path--220 feet--for the secondaries, then the e, π, K and p bunches from a particular primary electron bunch will arrive at different times. The electrons will take approximately 220 nsec to travel from target to detector. The π, K, and p bunches will arrive 0.015 nsec, 0.19 nsec, and 0.68 nsec later. In other words the π, K, and p bunches will lag behind the secondary

electron bunches by 15, 195, and 705 deg of phase, respectively. The DCFEM will therefore "see" the electrons and pions bunched together, the kaons about 180 deg of phase apart, and, since the protons lag by close to two full cycles, they will appear at nearly the same phase as the electrons and pions.

Figure 10 illustrates the time-of-flight separation of the various positively charged particles at 12 GeV/c. We see, as expected, that the K and π bunches are separated by 180 deg, and that the p and π bunches are very close in phase. An rf separator could take advantage from this situation, rejecting both π^+ and p in favor of K^+.

Thus in the K-π separation we have measured a time-of-flight difference of 0.17 nsec in a total time-of-flight of about 220 nsec.

B. Yields

All results are shown in Table I. The measurements have been corrected for scattering and interaction losses in the material of our counter array, and for the decay of pions and kaons in their flight from target to detector. The scattering and interaction corrections were typically 15%. To the statistical error associated with each measurement we have added algebraically an error of $\approx 2\%$, which reflects non-statistical fluctuations of unknown origin in the ratio of $S_1S_2S_3$ to monitor charge integral.

If the ratio of any two numbers in Table I that are associated with the same target is taken, then the error in that ratio is correctly obtained from the errors in the table. If the ratio of two numbers associated with different targets is taken, then an additional error of 3%

must be added to the error from Table I due to uncertainty in the ratio of beam monitor efficiency for the different targets (see Sec. II. A).

We believe that the overall normalization of the data is accurate to ± 15% (5% from beam monitor current normalization and 10% from solid angle and momentum bite uncertainty). That is, a lone number taken from Table I must have an additional 15% error added to compare with any absolute prediction.

Figures 11, 12, 13, and 14 show the 2-degree yields from Be at 18-GeV primary energy as a function of secondary momentum for $e^{\pm}$, $\pi^{\pm}$, $K^{\pm}$, and $p^{\pm}$. Figures 15, 16, and 17 show representative angular distributions of yields from 18-GeV primary electrons. In Fig. 15 the two points at 0.5 and 1 deg were taken from Boyarski et al.[13] It was necessary to correct their data from 16- to 18-GeV primary energy as well as to correct for a different target length (0.6 radiation length). The details of this conversion calculation are given in Sec. V. G. Comparison with the 0-deg data of Barna et al.[14] is not shown, since rather large and uncertain normalization factors would be needed to convert their 1.8-radiation-length data to a 0.3 radiation length.

The relationship between results from the Be target and results from the Fe target gives some indication about the dependence of the yields on the characteristics of the nucleus in the target. If we assume that the cross section (σ) for production of secondaries is proportional to A^n, where A is the atomic weight of the nucleus, then an expression for n in terms of the yields is

$$n = 1 + \ell n\,(r_B Y_F / r_F Y_B) / \ell n\,(A_F / A_B)\ ,$$

where r_B (r_F) is the radiation length of Be (Fe) in g/cm^2, and A_B (A_F) is the atomic weight of Be (Fe). Thus a given ratio of yields corresponds uniquely to a value for n. Of course, there is no guarantee that the cross section is proportional to any one power of A. In fact, it might depend on Z rather than on A, as elastic electron scattering does. However, this technique at least allows us to discuss the dependence of the yields on the target nucleus in Sec. V. F. Figure 18 shows the results for the ratio of yields from Be and Fe, along with the scale of n corresponding to each ratio.

The ratios of yields from the Be-Fe-combination target and the Be target are shown in Fig. 19. We note that adding a 1-cm length of iron to a 10-cm Be target increases the yields by a factor of 2 or 3. The significance of these results is discussed in Sec. V. B.

V. THEORETICAL INTERPRETATION OF YIELD RESULTS

A. Introduction

It is generally believed that production of strongly interacting particles (SIP) by an electron beam is a two-step process, with the electrons forming real photons by the bremsstrahlung process, followed by the interaction of the photons with the target nuclei. The analogous process with a virtual photon, usually called electroproduction, is important only for targets very much shorter than ours. Consideration of the two-step process allows us to roughly predict the dependence of yields on primary electron energy and on target length, and also derive some rough cross sections, as discussed in Sec. V. B.

Since real photons are incident on the nuclei, we need a theory of the photon-nucleus interaction to interpret the SIP yields; the mechanisms considered in this section are the Drell mechanism, ρ-meson production (for pions), and photodisintegration (for protons). The results, discussed in Sec. V.C and D, indicate that the pion, kaon, and anti-proton yields are explained, roughly, by the Drell and ρ processes, but the proton yields could be explained by the combination of Drell and photodisintegration processes.

We have obtained some yields for particles that are not strongly interacting: namely, electrons. In Sec. V.E, we have attempted to calculate the electron yields from elastic scattering of the incoming electrons, either with the nucleus as a whole, or with individual nucleons inside the nucleus. We find that the calculated yields are only about one-fifth the observed yields, indicating that inelastic processes, such as pion production, are dominating the electron scattering in this region of energy and angle.

Finally, we compare our results from the iron and beryllium targets in terms of the dependence of the yields on A, the atomic weight of the nucleus, in Sec. V.F.

B. Implications of the Bremsstrahlung Spectrum

As the primary electron beam proceeds through the Be target it creates real photons of a known energy spectrum and intensity. Calculations of the number of photons in a given energy interval, and at a given depth in the target, have been done by Tsai and Whitis.[15] If we knew the cross section for a photon producing a particular secondary particle

as a function of photon energy, then we could combine our knowledge of the photon spectrum with this cross section to produce a yield. This is what Tsai and Whitis have done with the Drell mechanism and ρ production cross sections treated in the next section.

However, suppose we know nothing about the cross section except the obvious fact that a photon with momentum p cannot produce a secondary particle with energy greater than p. Figure 20 illustrates the bremsstrahlung spectra integrated over the length of Be in the target, for three cases.

First let us compare curves (b) and (c). The path length of photons is much greater in the long target than in the shorter one, but the shapes of the energy spectra are quite similar. Therefore we expect the relative yields to be rather independent of specific production mechanisms; the yield of 10-GeV secondaries produced in the long and short targets should be roughly in proportion to the integral of curves (b) and (c) in Fig. 20 above 10 GeV/c. Table II and Fig. 19 show a comparison between predictions for the ratios of Be and Be-Fe yields and the experimental results for the SIP. We see that rough agreement is obtained.

Second we compare curves (a) and (c). Here the photon path-length distribution for 18-GeV electrons differs from that for 16-GeV electrons only in the 16-18 GeV region. Thus if the cross section for producing a certain secondary varies rapidly with photon energy, we would not expect the method of integrating the path length over energy to give an accurate prediction. However, the comparison between predictions for the ratios of 18 GeV and 16 GeV yields and the experimental results, shown in Table III, again indicates rough agreement. This

seems to indicate that the cross sections are relatively constant as a function of photon energy.

We have used this theory to convert the data given in Ref. 11 for 10-GeV/c π^+ yields, in order to plot their results in Fig. 15. We have converted from their 16-GeV electron beam to our 18-GeV electron beam (a factor of 1.3), and from their 0.6 r.l. target to our 0.3 r.l. target (a factor of 0.30), so that we multiplied their data at both 0.5 and 1 deg by 0.38. From our conclusions above we estimate the error in this conversion factor to be less than 30%.

By subtracting the yields of 16-GeV electrons from the yields of 18-GeV electrons, we can form a crude idea of the actual cross sections for secondary-particle production by monochromatic 17-GeV photons. The integrated path length for the difference is $\approx 3.6 \times 10^{-3}$ r.l./electron, which means that a difference between 18 and 16 GeV yields of 1 particle $\text{GeV}^{-1}\ \text{sr}^{-1}\ (10^7 \text{ incident electrons})^{-1}$ from the Be target represents a cross section of 7 μb $\text{sr}^{-1}\ (\text{GeV/c})^{-1}$. For example, the cross section for 3 deg production of 12-GeV/c π^- by 17-GeV photons on Be is 0.1 mb $\text{sr}^{-1}\ (\text{GeV/c})^{-1}$. For comparison we note that the cross section for 0 deg (5 deg) production of 12-GeV/c π^- by 18.8-GeV protons[16] on Be is 17 (0.2) mb $\text{sr}^{-1}\ (\text{GeV/c})^{-1}$.

C. Predictions of Drell + ρ for π, K, p, and $\bar{p}$ Yields

Calculations of the yields of pions and kaons from the Drell process, and also of the pion yields from ρ-meson production, have been performed by Tsai and Whitis.[17] Their results at 2 deg and as a function of secondary momenta, shown in Figs. 12 and 13, give order-of-magnitude agreement with the experimentally observed yields. Their prediction

of the angular distributions at fixed secondary momenta, shown in Figs. 15 and 16, are similar to the observed angular distributions, except that the experimental distributions seem to decrease with increasing angle less rapidly than the theoretical ones.

Both the Drell and ρ processes predict that the ratio of the yields of π^+ and π^- is unity for all secondary momenta. This is observed experimentally. However, the Drell process predicts that K^+/K^- is 1.3, but the observed ratio varies between 1.6 and 3.7. This appears to imply that the process $\gamma p \rightarrow K^+ \Lambda (\Sigma)$ is important; however, this process has been calculated[6] to be 2 to 3 orders of magnitude lower than necessary to explain the observed excess of K^+ over K^-. Another process[6] which could produce more K^+ than K^- is $\pi p \rightarrow K^+ \Lambda (\Sigma)$ taking place inside the same nucleus in which the π is produced by a γ. Although data on the A dependence of the yields should shed light on this possibility, the results in Sec. V.F are not accurate enough to confirm or disprove that K^+'s are being produced by pions.

The quantitative disagreement between Drell + ρ and experiment in the dependences of π and K yields on secondary momentum and production angle may be understood qualitatively by invoking one other mechanism: final-state interactions. If, after the Drell process has operated to produce a π or K, the π or K interacts with the rest of the nucleus, two effects will occur: (a) the angular distribution of the secondary particle will be broadened by scattering, and (b) the distribution of momenta of the secondary particle will favor lower momenta than the simple Drell process would indicate, because of energy loss in the scattering. These two effects, qualitatively, are indeed seen.

The $\bar{p}$ yields, shown in Fig. 14, are consistent with the order-of-magnitude prediction of the Drell mechanism. However, the Drell process predicts that $p/\bar{p}$ is 1, whereas experimentally we have $p/\bar{p} \approx 10$. Hence some other mechanism is operating in the proton case. A possibility, photodisintegration, is discussed in Sec. V.D.

Hence the $\pi^{\pm}$, K^-, and $\bar{p}$ yields are qualitatively explained by the combination of the Drell process and ρ production, with the addition of final-state interactions. We are forced to say "qualitatively" presumably only because we cannot calculate the final-state interactions. The K^+ and p yields appear to have different mechanisms operating, in the K^+ case perhaps associated production by pions, and in the proton case perhaps photodisintegration.

D. Proton Yields - Photodisintegration

The Drell mechanism, in fact just about any mechanism by which a proton-antiproton pair is created, predicts equal yields for protons and antiprotons. The antiproton yields are a reasonable order-of-magnitude for the Drell process, but the proton yields, shown in Fig. 14, are an order-of-magnitude higher.

Drell has suggested that photodisintegration can account for the proton yields.[7] In this mechanism, the photon finds a proton with a very large momentum inside the nucleus, and can thus produce a proton with large momentum transfer without depressing the amplitude with a small form factor. This model therefore depends crucially on the probability of the photon's finding a proton with high momentum in the nucleus; in other words, it depends crucially on what is assumed for the wave function of the nucleus.

Extremely rough calculations[18] indicate the following: If an exponential wave function is assumed, there are enough high-momentum components to predict a proton yield of the right order-of-magnitude. However if a shell-model wave function is assumed, then the amount of high-momentum components is entirely too small to account for the observed yields.

Until more is known about the nuclear wave functions we can only guess that photodisintegration, or similar processes which might produce some extra pions but do not produce antiprotons, are active here.

E. Electron Yields

The mechanism for producing secondary electrons is quite different from that which produces SIP. First we realize that electrons of all energies are produced in the forward direction as the primary electrons lose energy by bremsstrahlung. However, neither the bremsstrahlung process nor multiple scattering in the target is capable of sending secondary electrons off at angles of 2 or 3 deg. Only a single strong collision of the secondary electron with one nucleus is capable of yielding significant amounts of secondary electrons at large angles.

It is tempting to predict that among the single-scattering events, only elastic scattering, either off the nucleus as a whole (coherent), or off a single nucleon within the nucleus (incoherent), is important. If that were the case then we could describe the production of secondary electrons in the following way: A primary electron enters the target and gradually loses energy by bremsstrahlung radiation until it emerges at the end of the target with the secondary momentum we are studying (the probability that the electron will emerge with any given momentum has

been calculated). Somewhere along its path through the target the electron suffered an elastic collision (no energy loss) that provided a sufficient impulse for it to emerge from the end of the target at a production angle of 2 (or 3) degrees.

To calculate the yields from this whole process, we first need the elastic electron-nucleus scattering cross section which is

$$\frac{d\sigma}{d\Omega} = F^2 \left(\frac{d\sigma}{d\Omega}\right)_{Ros}$$

where $\left(\frac{d\sigma}{d\Omega}\right)_{Ros}$ is the Rosenbluth cross section, and

$$F^2 = Z\, F_p^2 + Z\,(Z - 1)\, F_{Be}^2$$

$$F_p = 1/(1 + 1.4\, Q^2)^2$$

$$F_{Be} = 1/(1 + 26\, Q^2)\,,$$

where Q^2 is the four-momentum transfer in $(GeV)^2$ (form factors are from Ref. 19).

We now make the reasonable approximation, for electrons emerging from a target of length t_0 with energy E_f, that their energy as a function of depth in the target is

$$E(t) = E_0 \left(\frac{E_f}{E_0}\right)^{\alpha}$$

where $\alpha = t/t_0$, and E_0 is the primary electron energy (this equation is exact on the average but of course is not true for each individual electron). Then the effective cross section for a single scatter is

$$\left(\frac{d\sigma}{d\Omega}\right)_{eff} = \int_0^1 \frac{d\sigma(E)}{d\Omega}\, d\alpha\,.$$

This integration has been carried out for the Be target and a production angle of 2 deg, and the result is presented as the curve in Fig. 11. We see that the theory is a factor of ≈5 too low. We must conclude that other single-scattering processes are dominating the electron yields (e.g., single-pion production).

F. General Interpretation of A Dependences

Since we obtained data from targets of Be and Fe with the same radiation length in each, we have a measure of the dependence of the yields on A, as explained in Sec. IV.B. It is rather presumptuous of us to take two points from a perhaps complicated curve, and connect them with a straight line, but lacking more information we hope we can deduce something of value from this approximation.

The pion results are shown in Fig. 18(b). We note that the π^+ and π^- results are identical within errors, a reflection of the fact that the yields of π^+ and π^- are equal for both the Fe and Be targets. We also note that n is tending to a value less than 0.8 at high energy. We can understand this in the following way: Any pion which is formed inside a nucleus must progress through nuclear matter, where it has a good chance of interacting on its way out. For pions produced with the maximum possible energy, only those that are produced on the back surface of the nucleus will be able to escape with no loss of energy. Hence the high-energy limit of n in Fig. 18(b) should be 0.67. The Drell mechanism predicts 0.67 also, but for all energies, because the "almost real" pion interaction with the nucleus should have the same A dependence as a real pion interaction. However, models have shown that the virtuality of the exchanged pion can change the A dependence.[20]

The K and p results are shown in Fig. 18(c) and (d). We evidently must restrict ourselves to saying that roughly $\frac{2}{3} < n < \frac{4}{3}$. We would wish to have better results in the K case, since we might then reach a conclusion as to whether K^+'s are produced by $\pi p \rightarrow K^+ \Lambda (\Sigma)$ inside nuclei where pions are formed, but our data are insufficient.

The electron results are shown in Fig. 18(a). Here we do not expect the cross section to depend on A but rather on Z. However, since $A_{Be}/A_{Fe} = Z_{Be}/Z_{Fe}$, we can regard n as a power of Z. We see that n is between 1 and 2 but closer to 1, which we interpret to indicate that coherent nuclear interactions are taking place but incoherent processes are dominant.

The shape of the "A dependence" curve as a function of energy, which is well determined for e and π, remains to be explained quantitatively.

ACKNOWLEDGMENTS

We thank Roger A. Gearhart and Todd Hauser of the Lawrence Radiation Laboratory for their great efforts in the preparation and running of the experiment. We wish to express appreciation to the University of Hawaii Physics Department for its interest and help during the experiment.

We are grateful to many people at the Stanford Linear Accelerator Center, but especially to Dr. Y. S. Tsai and V. Whitis for their extensive theoretical calculations, and Professor S. D. Drell for several stimulating discussions. We wish to thank the Research Area Department for skillful operation of the accelerator and associated equipment. The assistance and cordiality of the entire SLAC staff is gratefully acknowledged.

Finally, it is a pleasure to thank Professor Luis Alvarez for his encouragement and support.

FOOTNOTES AND REFERENCES

*This work was done under the auspices of the U. S. Atomic Energy Commission.

†Now at Stanford Linear Accelerator Center, Stanford University, Stanford, California.

1. S. D. Drell, Phys. Rev. Letters 5, 278 (1960).
2. W. A. Blanpied, J. S. Greenberg, V. W. Hughes, D. C. Lee, and R. C. Minehart, Phys. Rev. Letters 11, 477 (1963); R. B. Blumenthal, W. L. Faissler, P. M. Joseph, L. J. Lanzerotti, F. M. Pipkin, D. G. Stans, J. Ballam, H. De Staebler, Jr., and A. Odian, Phys. Rev. Letters 11, 496 (1963).
3. J. S. Ballam, M Report No. 200, W. W. Hansen Laboratories of Physics, Stanford University, 1960 (unpublished); S. D. Drell, Rev. Mod. Phys. 33, 458 (1961); for a more recent review see Drell's article in Proceedings of the International Symposium on Electron and Photon Interactions at High Energies, Hamburg, 1965 (Springer-Verlag, Berlin, 1965), p. 71.
4. S. M. Berman and S. D. Drell, Phys. Rev. 133, B791 (1964).
5. S. M. Flatté, R. A. Gearhart, T. Hauser, J. J. Murray, R. Morgado, M. Peters, P. R. Klein, L. H. Johnston, and S. G. Wojcicki, Phys. Rev. Letters 18, 366 (1967).
6. Y. S. Tsai, Stanford Linear Accelerator Center Users Handbook (unpublished).
7. S. D. Drell, Stanford Linear Accelerator Center, private communication.

8. R. A. Gearhart, T. Hauser, L. H. Johnston, P. R. Klein, and J. J. Murray, A Target Beam Monitor Using Secondary Electron Emission (to be submitted to Rev. Sci. Instr.).

9. O. L. Gaddy and D. F. Holshouser, Proc. IEEE 51, 153 (1963).

10. T. F. Kycia and E. W. Jenkins, in Proceedings of the Conference on Nuclear Electronics, Belgrade, 1961 (International Atomic Energy Agency, Vienna, 1962), Vol. I, p. 63.

11. S. M. Flatté, R. A. Gearhart, T. Hauser, P. R. Klein, J. J. Murray, and S. G. Wojcicki, A Microwave-Gated Photomultiplier Tube (to be submitted to Rev. Sci. Instr.).

12. G. Loew, Stanford Linear Accelerator Center, private communication.

13. A. Boyarski, F. Bulos, W. Busza, D. Coward, R. Diebold, J. Litt, A. Minten, B. Richter, and R. Taylor, Phys. Rev. Letters 18, 363 (1967).

14. A. Barna, J. Cox, F. Martin, M. L. Perl, T. H. Tan, W. T. Toner, and T. F. Zipf, Phys. Rev. Letters 18, 360 (1967).

15. Y. S. Tsai and V. Whitis, Phys. Rev. 149, 1250 (1966).

16. D. Dekkers, J. A. Geibel, R. Mermod, G. Weber, T. R. Willitts, K. Winter, B. Jordan, M. Vivargent, N. M. King, and E. J. N. Wilson, Phys. Rev. 137, B962 (1965).

17. Y. S. Tsai and V. Whitis, Stanford Linear Accelerator Center, private communication.

18. J. Gillespie, Stanford Linear Accelerator Center, private communication.

19. R. Hofstadter, Ann. Rev. Nucl. Sci. 7, 231 (1957).

20. J. S. Bell, Phys. Rev. Letters 13, 57 (1964).

Table I. Particle yields in particles $sr^{-1}(GeV/c)^{-1}$ per 10^7 incident electrons. Both the Be and Fe targets were 0.3 radiation length, but the Be-Fe target consisted of 0.6 r.l. of Fe followed by 0.3 r.l. of Be. The errors reported here are the algebraic sums of the statistical errors and nonstatistical fluctuations described in the text. The overall normalization of the data is believed to be accurate to ± 15%. All yields are at the target, i.e., they have been corrected for decay-in-flight. The muon fraction, measured at a few momenta, was found to be < 1% of the total yield.

Target, primary electron energy, and production angle	Charge and secondary momentum (GeV/c)	Yield			
		Electron	Pion	Kaon	Proton
Be	+10		148 ± 6	26 ± 3	10.7 ± 1.7
16 GeV[a]	+12		35.2 ± 1.6	10.7 ± 1.2	3.2 ± 0.3
3 deg	-10	252 ± 12	156 ± 11	10.7 ± 1.2	1.1 ± 0.2
	-12	299 ± 9	37 ± 4	2.8 ± 0.4	0.17 ± 0.10
Be	+6		1480 ± 60	103 ± 15	126 ± 30
18 GeV[b]	+10		186 ± 8	35 ± 3	15.1 ± 1.8
3 deg	+12		64 ± 3	14.2 ± 1.7	8.0 ± 0.9
	-12	164 ± 5	52 ± 3	4.3 ± 0.5	0.26 ± 0.07
Be	+4	440 ± 40	2330 ± 100	230 ± 30	260 ± 80
18 GeV[b]	+6	98 ± 12	2130 ± 60	166 ± 21	84 ± 10
2 deg	+8		1630 ± 40	86 ± 11	49 ± 4
	+10		900 ± 20	56 ± 3	23.2 ± 1.7
	+12[c]		304 ± 7	31 ± 3	9.8 ± 0.8
	+14		76 ± 2	14.6 ± 1.5	3.5 ± 0.6
	-4	2780 ± 120	2520 ± 150	114 ± 10	
	-6	1280 ± 80	2050 ± 100	103 ± 11	7.1 ± 1.3
	-8	970 ± 60	1680 ± 80	49 ± 5	5.1 ± 1.0
	-10	970 ± 50	820 ± 50	22.5 ± 2.5	2.9 ± 0.7
	-12	930 ± 40	280 ± 30	8.3 ± 0.9	1.2 ± 0.4
	-14	1060 ± 40	74 ± 26	4.5 ± 0.7	
Fe	+4	226 ± 18	503 ± 27	65 ± 8	82 ± 22
18 GeV[b]	+6	28 ± 3	512 ± 13	40 ± 5	20 ± 2
2 deg	+8		517 ± 12	24 ± 3	11 ± 1
	+10		306 ± 6	14 ± 1	5.4 ± 0.5
	+12		57 ± 1.4	6.2 ± 0.7	1.6 ± 0.25
	+14		12.2 ± 0.5	3.7 ± 0.5	0.55 ± 0.15
	-4	1410 ± 65	650 ± 70	49 ± 5	
	-6	400 ± 24	510 ± 30	25 ± 2.5	
	-8	320 ± 20	560 ± 30	15 ± 2	1.7 ± 0.3
	-10	275 ± 15	285 ± 20	4.3 ± 0.7	0.7 ± 0.2
	-12	286 ± 12	52 ± 8	2.1 ± 0.4	0.1 ± 0.1
	-14	316 ± 6			
Be-Fe	+6	580 ± 120	5410 ± 240	380 ± 50	170 ± 20
18 GeV[b]	+8		4930 ± 120	250 ± 30	146 ± 16
2 deg	+12		663 ± 17	71 ± 7	24 ± 2.5
	-6	4290 ± 260	5610 ± 330	230 ± 30	16 ± 2
	-12	1180 ± 60	580 ± 50	20 ± 3	1.9 ± 0.7

a. 16.00 ± 0.08 GeV

b. 17.85 ± 0.15 GeV

c. Deuterons here were found to be less than 3% of the protons

Table II. Ratios of yields from the Be-Fe target (0.6 r.l. Fe followed by 0.3 r.l. Be) to yields from the 0.3 r.l. Be target, with predictions calculated from the expected photon distributions in the target, as explained in Sec. V. B. The primary electron energy was 18 GeV, and the production angle was 2 deg.

Charge and secondary momentum (GeV/c)	(Be-Fe yield/Be yield)			
	Prediction	Experiment		
		Pion	Kaon	Proton
+6	2.84	2.5 ± 0.1	2.3 ± 0.4	2.0 ± 0.3
+8	2.64	3.0 ± 0.1	2.9 ± 0.5	3.0 ± 0.4
+12	2.24	2.2 ± 0.1	2.3 ± 0.3	2.5 ± 0.3
-6	2.84	2.7 ± 0.2	2.3 ± 0.4	2.3 ± 0.5
-12	2.24	2.1 ± 0.3	2.4 ± 0.4	1.6 ± 0.8

Table III. Ratios of yields from 18-GeV electrons to yields from 16-GeV electrons, with predictions calculated from the expected photon distributions in the target, as explained in Sec. V. B. The target was 0.3 r.l. of Be, and the production angle was 3 deg.

Charge and secondary momentum (GeV/c)	18-GeV yield/16-GeV yield			
	Prediction	Experiment		
		Pion	Kaon	Proton
+10	1.29	1.25 ± 0.1	1.35 ± 0.2	1.4 ± 0.3
+12	1.49	1.8 ± 0.1	1.35 ± 0.2	2.5 ± 0.4
-12	1.49	1.4 ± 0.2	1.55 ± 0.3	1.55 ± 1.0

FIGURE CAPTIONS

Fig. 1. (a) Beam configuration (not to scale). C1 and C2 are lead collimators. (b) Counter array (not to scale). S_1, S_2, S_3, S_4, and S_5 are plastic scintillators; C_1 and C_2 are respectively threshold and differential Čerenkov detectors; D1 and D2 are DCFEM's described in the text.

Fig. 2. Development of an electron shower as seen by the shower counter S_4. The S_4 voltage was set so that singles did not register at a 100-mV discriminator setting. The secondary beam momentum was 6 GeV/c, where the Čerenkov counters indicated that $44 \pm 2\%$ of the beam were electrons. The "plateau" with 7/8-in. Pb was poor because of the small multiplicity of the shower at this low energy.

Fig. 3. Discriminator curves on the "shower counter" S_4. The plateau at low discriminator settings gets increasingly better as the momentum of the secondary beam increases. (Also, by the way, the electron fraction in the beam rises above 8 GeV/c.) The length of Pb in front of S_4 varied from 7/8 in. at 4 GeV to 1 1/4 in. at 14 GeV.

Fig. 4. A measurement of the μ fraction in the +12-GeV/c secondary beam for 18-GeV electrons on the Be target at 2 deg. The counter S_5 was used with various thicknesses of Fe in front of it. The attenuation of SIP follows the expected straight line until the very last point, which is 0.6% above the extrapolated line. We conclude that the μ fraction here is $< 1\%$.

Fig. 5. The separation power of our Čerenkov counters. This data is for negatively charged particles. For data above the π peaks, C_1

was used to anti out the tails of the e and π peaks as well as to eliminate accidentals. The width of the peaks, 8 lb/in.^{2}, corresponds to a $\Delta\beta = 4 \times 10^{-4}$. From this raw recorded data, we can read directly the percentages of K, p, and, at the lower momenta, e and π in the beam.

Fig. 6. A schematic illustration of the DCFEM, a microwave-gated photomultiplier tube. (See text for details.)

Fig. 7. Gating properties of the DCFEM as calculated by computer simulation of the dynamics and the secondary emission process. The ordinate is the magnitude of the pulse put out by the tube as a function of the arrival phase (time during the rf cycle) of a photon incident on the photo-cathode.

Fig. 8. The detection efficiency of the DCFEM as a function of phase for 10-GeV electrons. The shape of this curve represents a folding of the DCFEM response curve (Fig. 7 put through a discriminator) and the shape of the electron bunch. The sharp edge puts a limit of 20 deg-of-phase on the electron-bunch width, as seen from the derivative curve (dashed line).

Fig. 9. Measurement of the fraction of electrons in the half-cycle away from the main bunch, with data from two DCFEM's in coincidence. When the DCFEM phase "window" is centered off the electron bunch, it detects $< 0.6 \times 10^{-3}$ of the electrons. This curve also sets an upper limit of 10 deg-of-phase on the electron bunch width (secondary beam).

Fig. 10. Time-of-flight measurements of π^+, K^+, and p at 12 GeV/c. The time-of-flight (modulo the rf period) of particles over the 220-ft

beam was measured with the DCFEM. The 12-GeV/c π^+ will take approximately 220 nsec to travel from target to detector. The K and p bunches will arrive 0.19 and 0.68 nsec later, or 195 and 705 deg-of-phase later, respectively. This figure shows the K and π peaks separated by $\approx$ 180 deg, and the p and π peaks separated by $\approx$ 0 deg in good agreement with expectations.

Fig. 11. Yields of $e^{\pm}$ for a 2-deg production angle and 18-GeV primary energy. Units are particles sr^{-1} $(GeV/c)^{-1}$ per incident electron on a 0.3-radiation-length Be target. Errors shown are the algebraic sums of the statistical errors and non-statistical fluctuations as described in the text. The overall normalization of the data is believed to be accurate to $\pm$ 15%. The dashed lines are to eliminate confusion. The solid curve is the result of a theoretical calculation taking into account elastic scattering of the primary electrons (off Be nuclei and individual nucleons within the Be nuclei), and the energy loss of the electrons as they traverse the target. (See Sec. V.E.) The much larger experimental yield ($\approx$ factor of 5) arises from inelastic scattering (e.g., single-pion production).

Fig. 12. Yields of $\pi^{\pm}$. The units, production angle, primary energy, target, and error determination are identical to those in Fig. 11. The solid curves are π yields from ρ production and from the Drell process, as calculated in Ref. 17.

Fig. 13. Yields of $K^{\pm}$. The units, production angle, primary energy, target, and error determination are identical to those in Fig. 11. The solid curve is the K^+ yield from the Drell process as calculated in Ref. 17; the K^- yields are everywhere 30% lower than K^+ yields calculated according to the Drell process.

Fig. 14. Yields of $p^{\pm}$. The units, production angle, primary energy, target, and error determination are identical to those in Fig. 11.

Fig. 15. Representative angular distributions for π^+ from 18 GeV primary electrons. The units, primary energy, target, and error determination are identical to those in Fig. 11. The 10-GeV/c distribution contains the adjusted data of Boyarski et al.[13] (see Sec. V.G.). The solid curves are π yields from the Drell process and from ρ production, as calculated in Ref. 17.

Fig. 16. Representative angular distributions of K^+. The units, primary energy, target, and error determination are identical to those in Fig. 11. The solid curve is the 10-GeV/c yield from the Drell process, as calculated in Ref. 17.

Fig. 17. Representative angular distributions of protons. The units, primary energy, target, and error determination are identical to those of Fig. 11.

Fig. 18. A dependences of the yields. The ratio of the Be-target yield to the Fe-target yield is plotted as a function of momentum for $e^{\pm}$, $\pi^{\pm}$, $K^{\pm}$, and p. On the assumption that the cross section for a photon on a nucleus, to produce a given particle, is proportional to A^n, where A is the atomic weight of the nucleus, there is a unique correspondence between a ratio and a value of n. The scale of n is shown on the right.

Fig. 19. Ratio of the Be-Fe-target yield to the Be-target yield, as a function of momentum, for π^+, K^+, and p. We note that adding a 1-cm thickness of iron to the front of a 10-cm thickness of Be increases the yield by a factor of 2 or 3. The continuous curves are

predictions based on the known photon spectra in the targets (see Sec. V. B).

Fig. 20. The photon-path-length spectra for electrons traversing different targets; (a) 16-GeV electrons through 0.3 r.l. of Be; (b) 18-GeV electrons traversing 0.6 r.l. of Fe followed by 0.3 r.l. of Be; (c) 18-GeV electrons traversing 0.3 r.l. of Be. "Path length" is a simple device for expressing the probability of a photon's being in proximity to a nucleus. To calculate a yield, one must fold in the (in general, energy-dependent) cross section for producing the particle of interest. A path length of 1 r.l. of Be is equivalent to 4.1 events/barn.

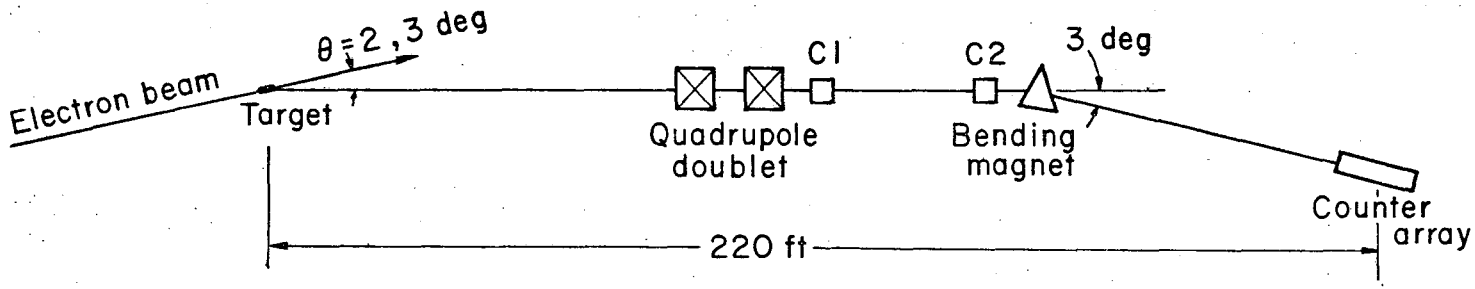

(a) Beam configuration

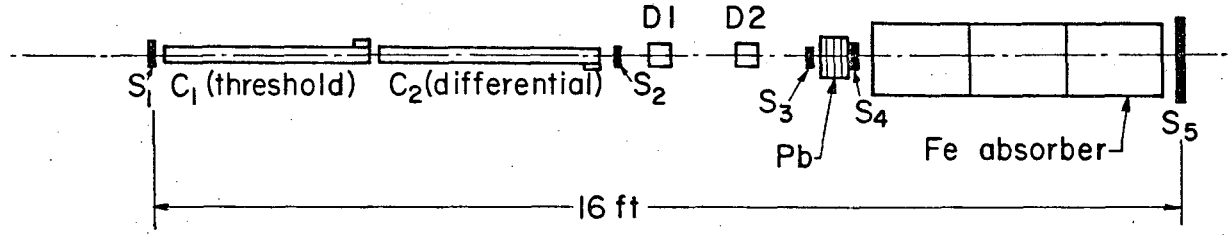

(b) Counter array

XBL671-318A

Fig. 1

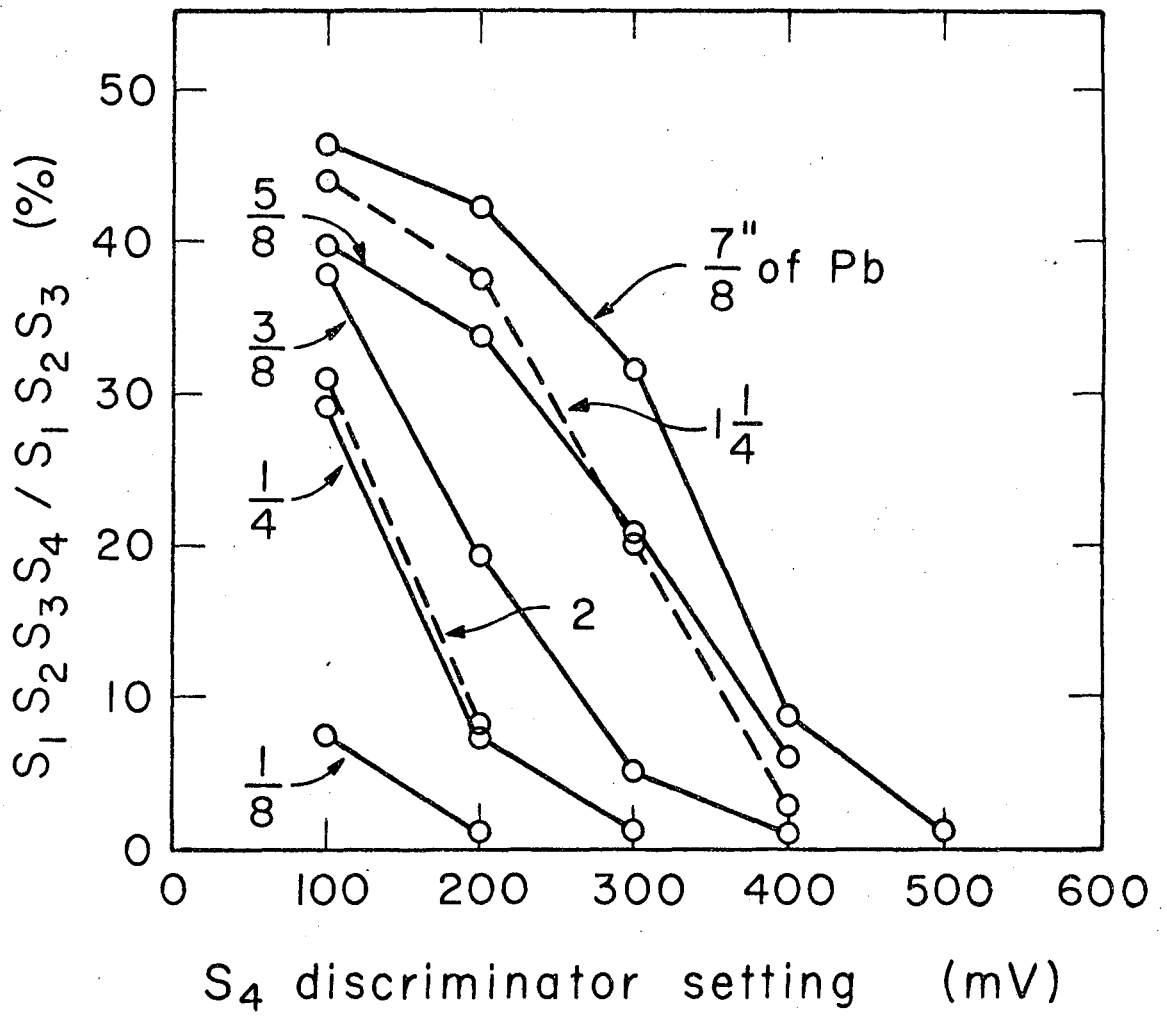

XBL677-3516

Fig. 2

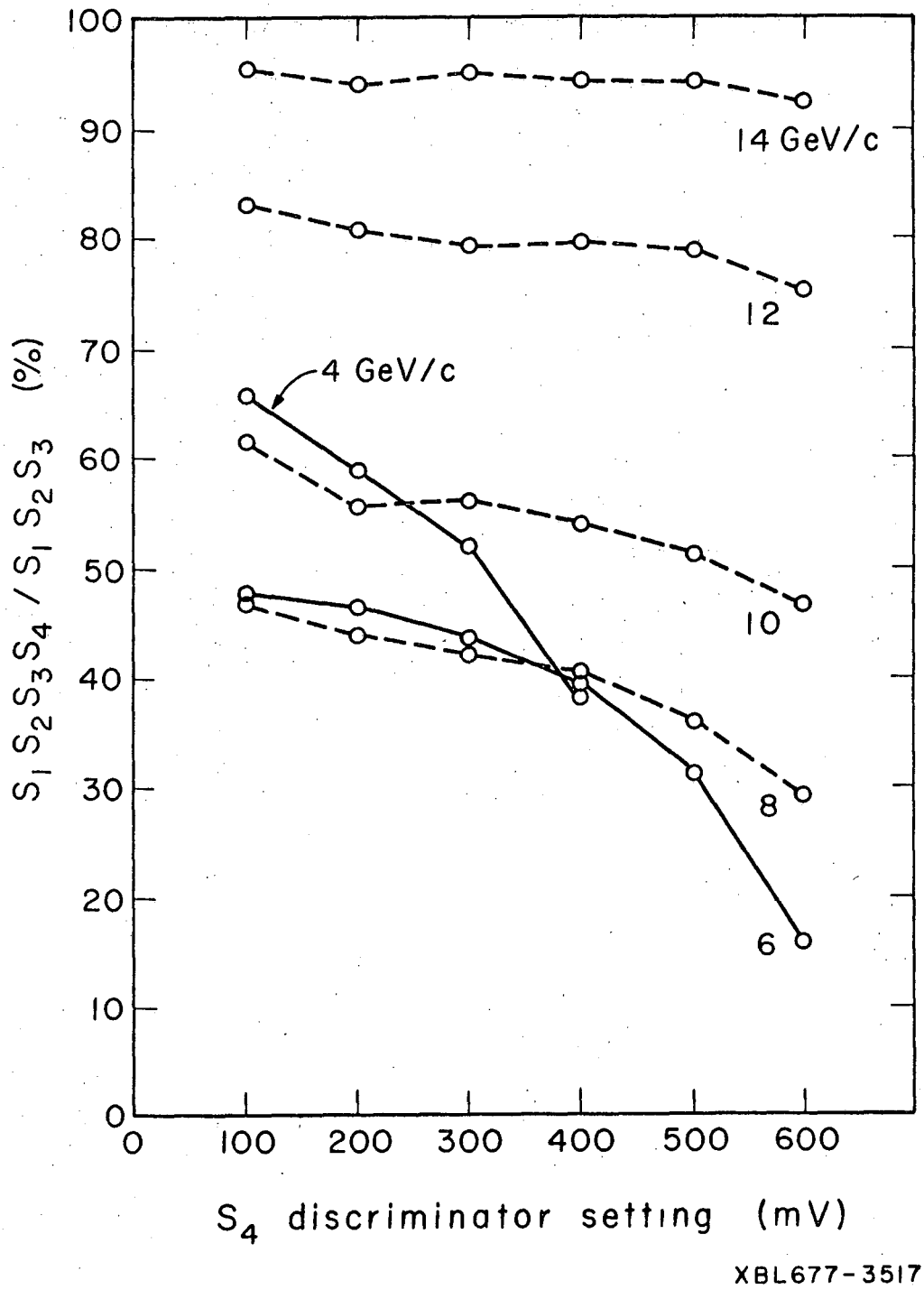
100
90
80
70
60
50
40
30
20
10
0
0
100
200
300
400
500
600
14 GeV/c
12
4 GeV/c
10
8
6
$S_1 S_2 S_3 S_4 / S_1 S_2 S_3$ (%)
S_4 discriminator setting (mV)
XBL677-3517

Fig. 3

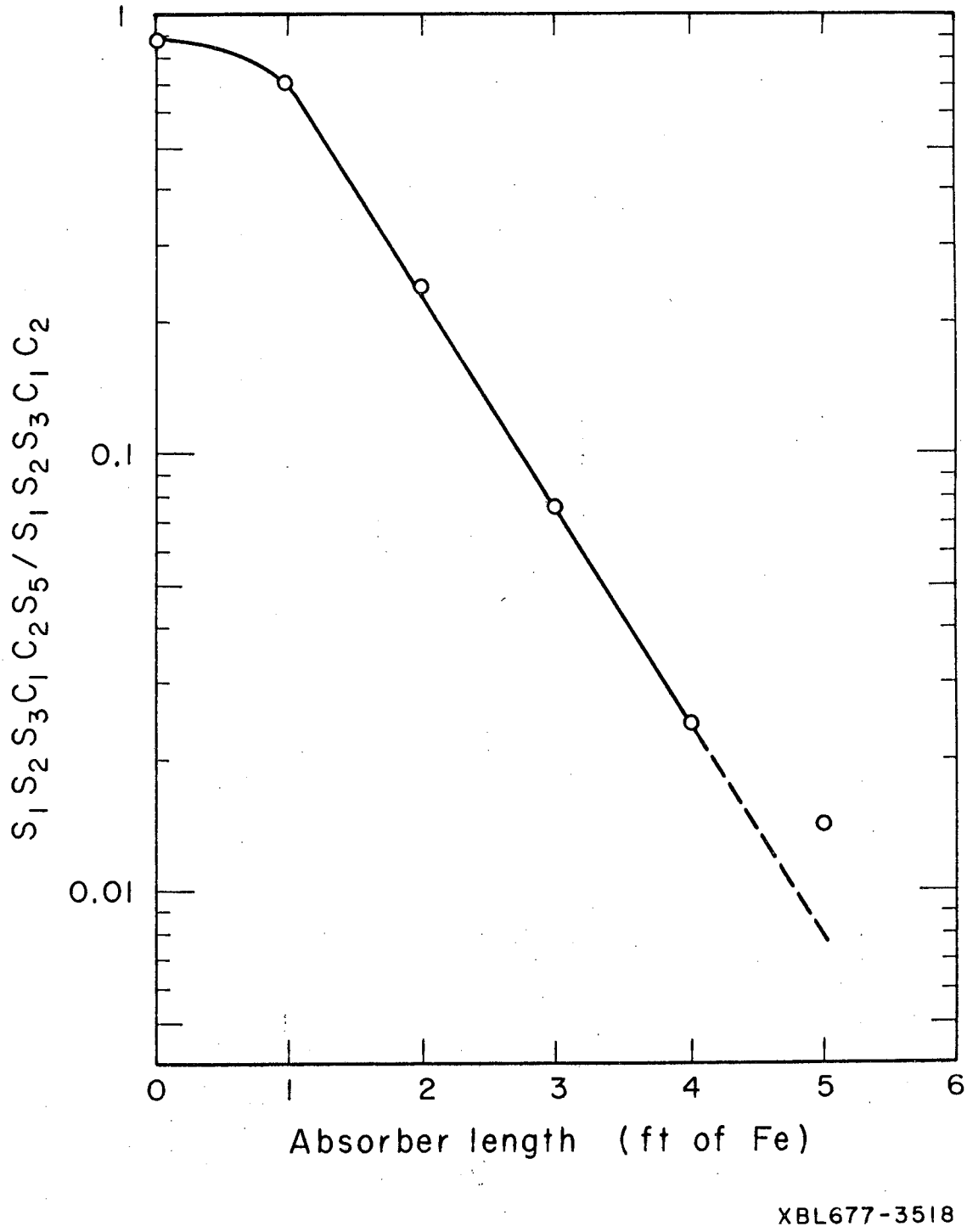
1
0.1
0.01
$S_1 S_2 S_3 C_1 C_2 S_5 / S_1 S_2 S_3 C_1 C_2$
0
1
2
3
4
5
6
Absorber length (ft of Fe)
XBL677-3518

Fig. 4

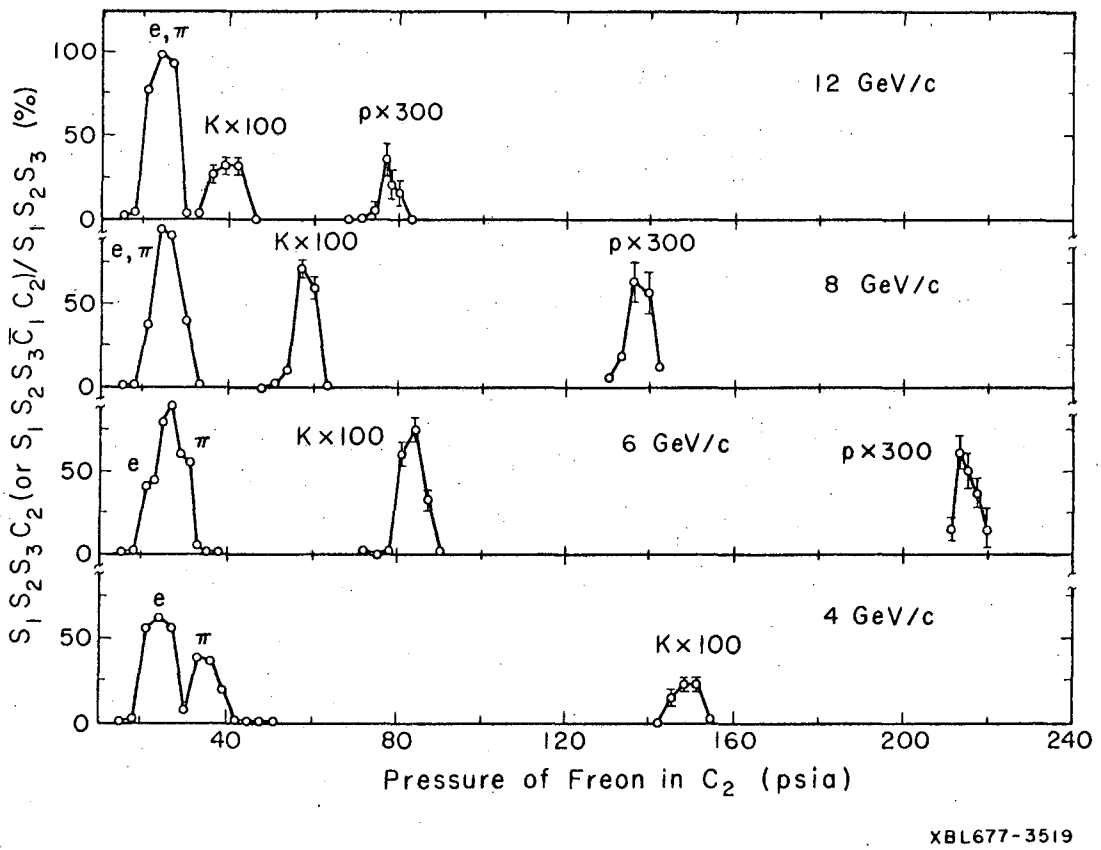
e, π
K×100
p×300
12 GeV/c
8 GeV/c
6 GeV/c
4 GeV/c
e
π
100
50
0
40
80
120
160
200
240
Pressure of Freon in C2 (psia)
S1 S2 S3 C2 (or S1 S2 S3 C̄1 C2)/S1 S2 S3 (%)
XBL677-3519

Fig. 5

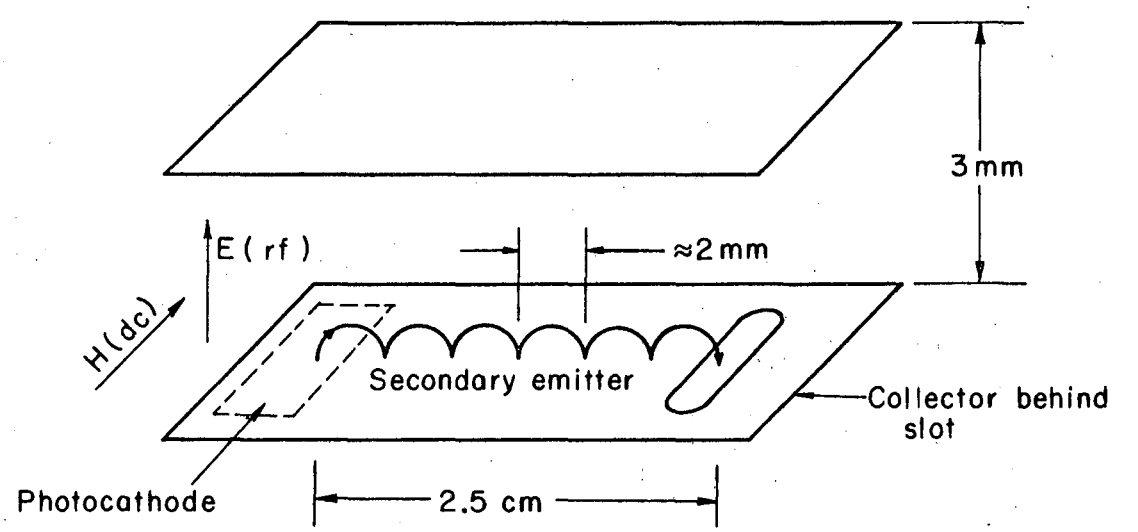
3 mm
E (rf)
≈2 mm
H(dc)
Secondary emitter
Collector behind slot
Photocathode
2.5 cm
MUB-12468A

Fig. 6

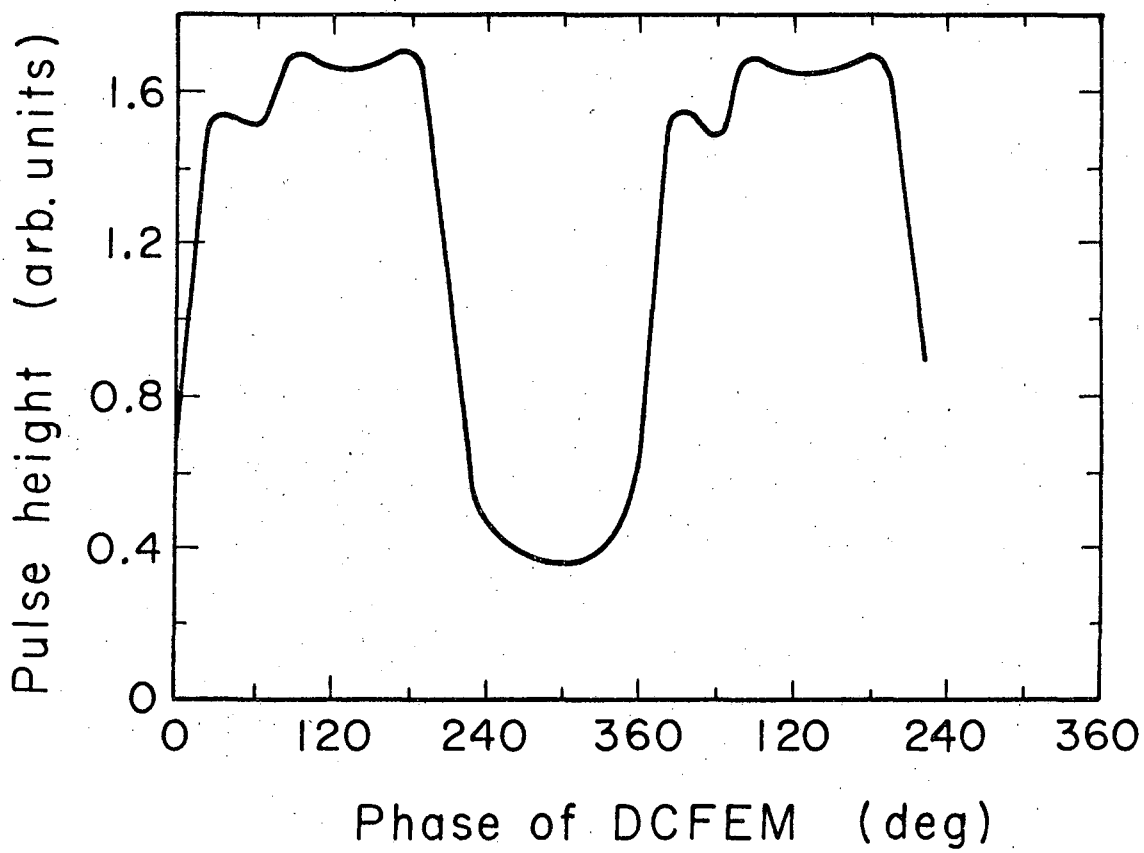

XBL677-3520

Fig. 7

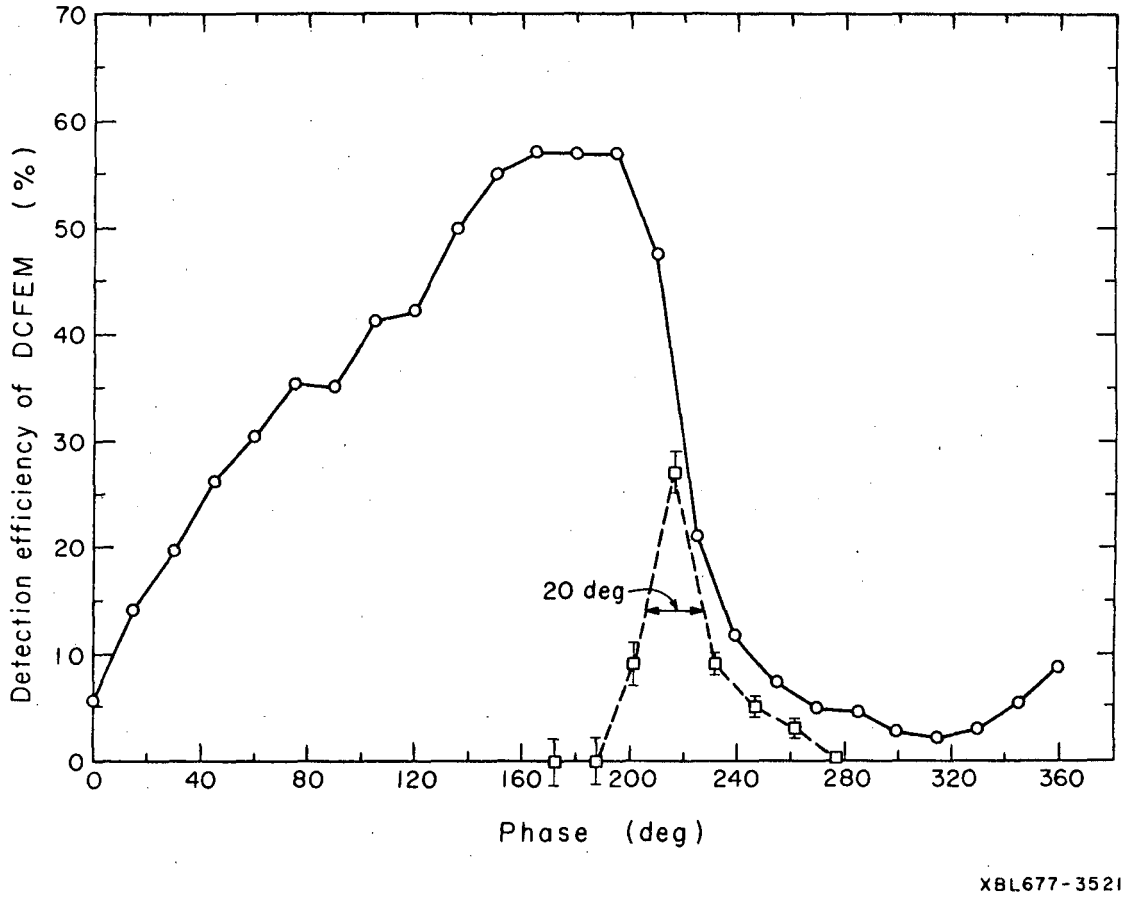
70
60
50
40
30
20
10
0
Detection efficiency of DCFEM (%)
20 deg
0
40
80
120
160
200
240
280
320
360
Phase (deg)
XBL677-3521

Fig. 8

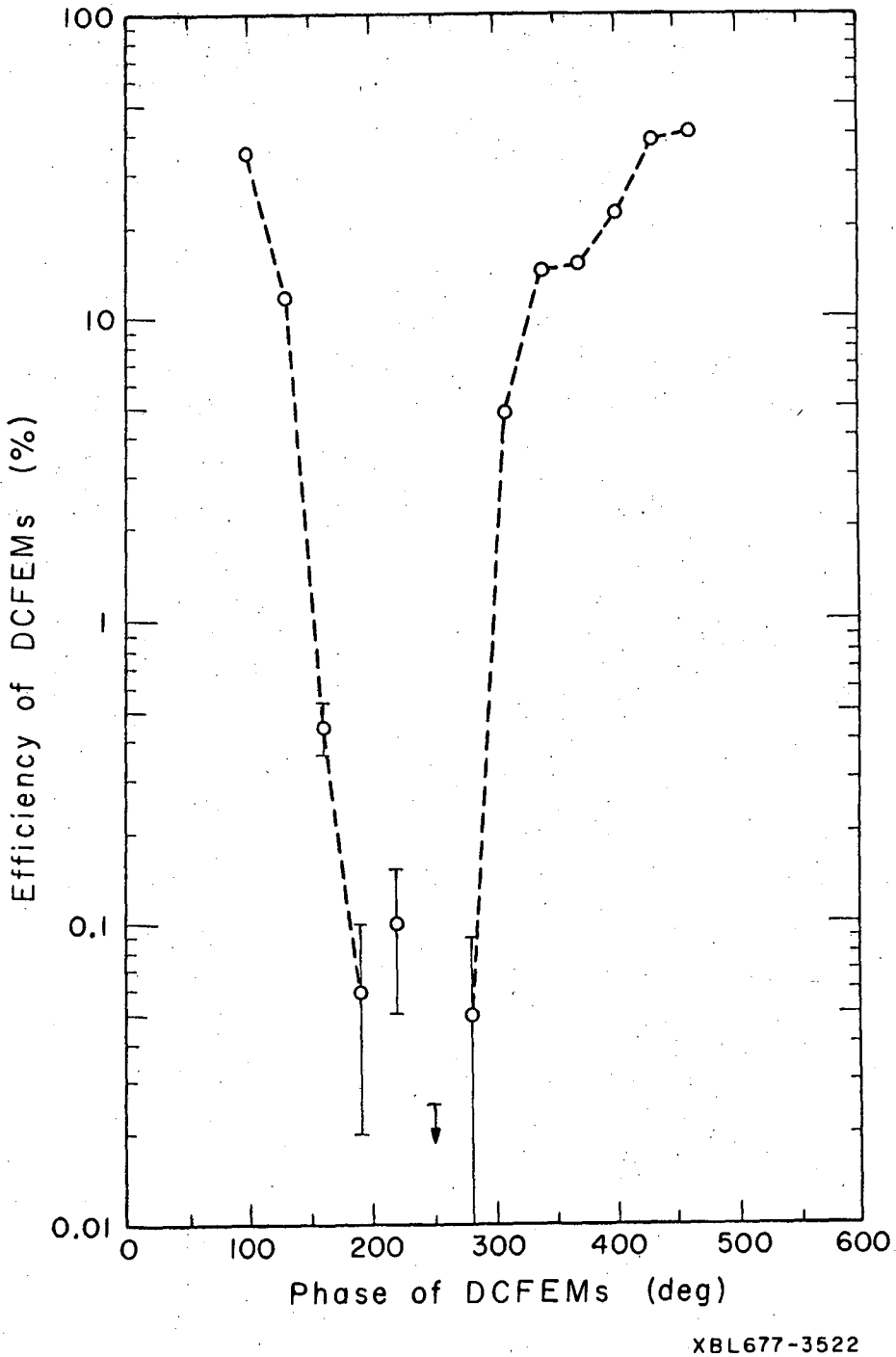
100
10
1
0.1
0.01
Efficiency of DCFEMs (%)
0
100
200
300
400
500
600
Phase of DCFEMs (deg)
XBL677-3522

Fig. 9

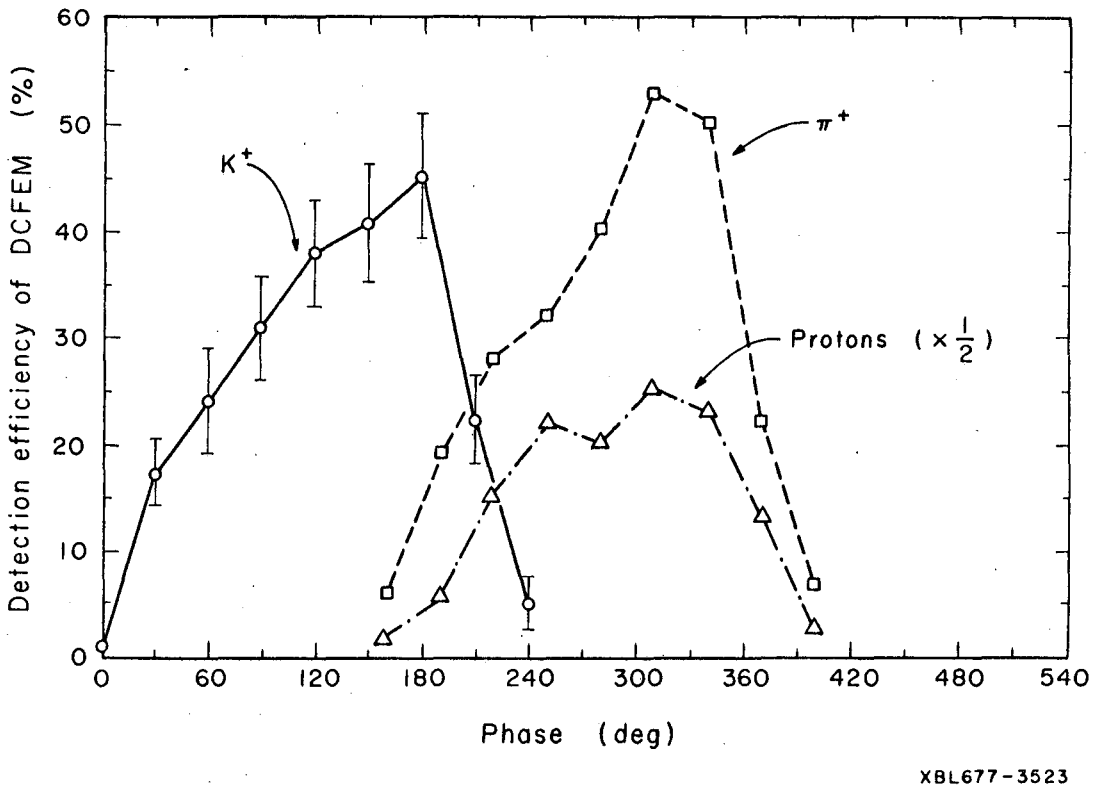
Detection efficiency of DCFEM (%)
60
50
40
30
20
10
0
0
60
120
180
240
300
360
420
480
540
Phase (deg)
K+
π+
Protons (× 1/2)
XBL677-3523

Fig. 10

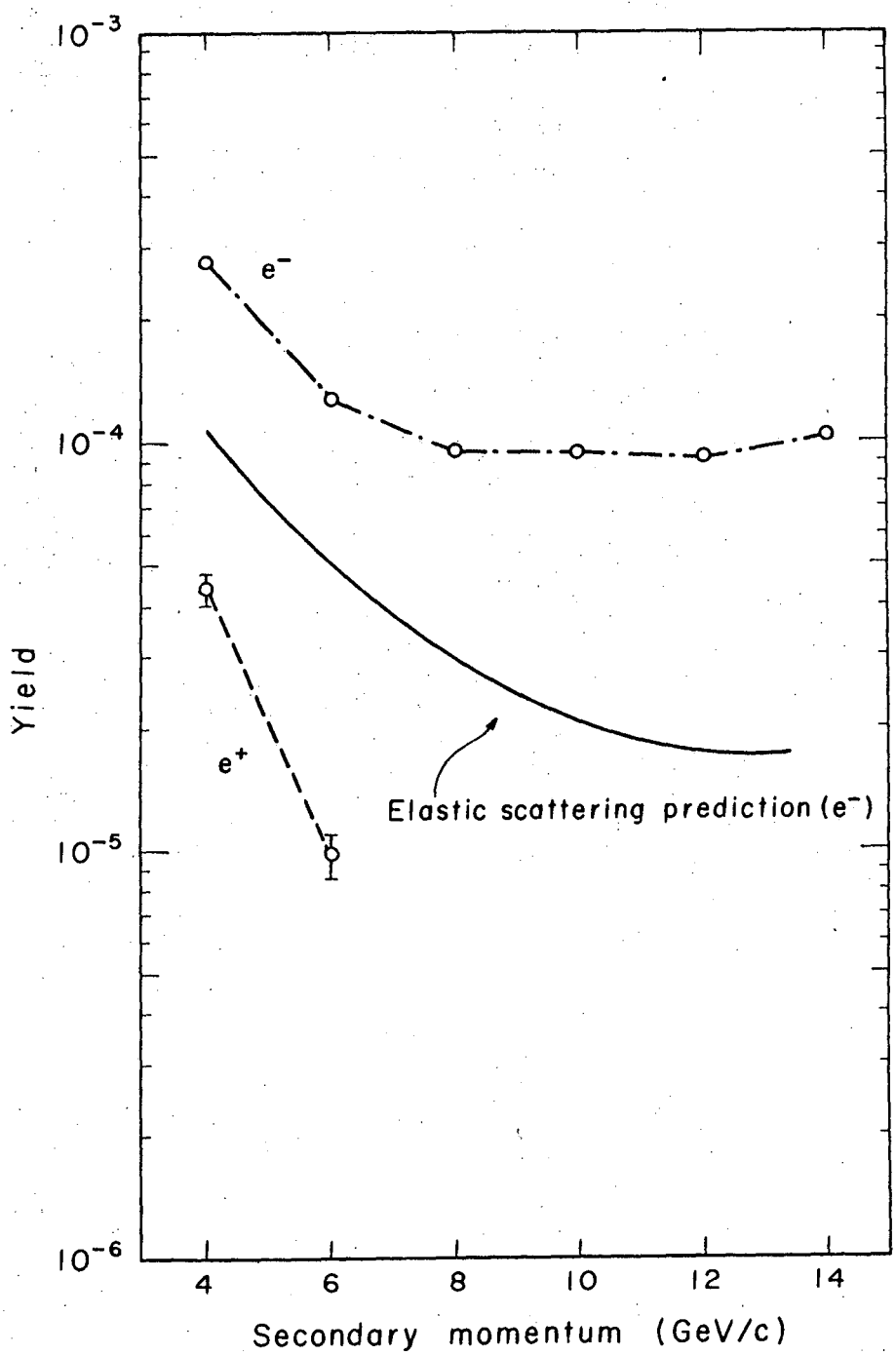
10^{-3}
10^{-4}
10^{-5}
10^{-6}
Yield
e^-
e^+
Elastic scattering prediction (e^-)
4
6
8
10
12
14
Secondary momentum (GeV/c)
XBL677-3524

Fig. 11

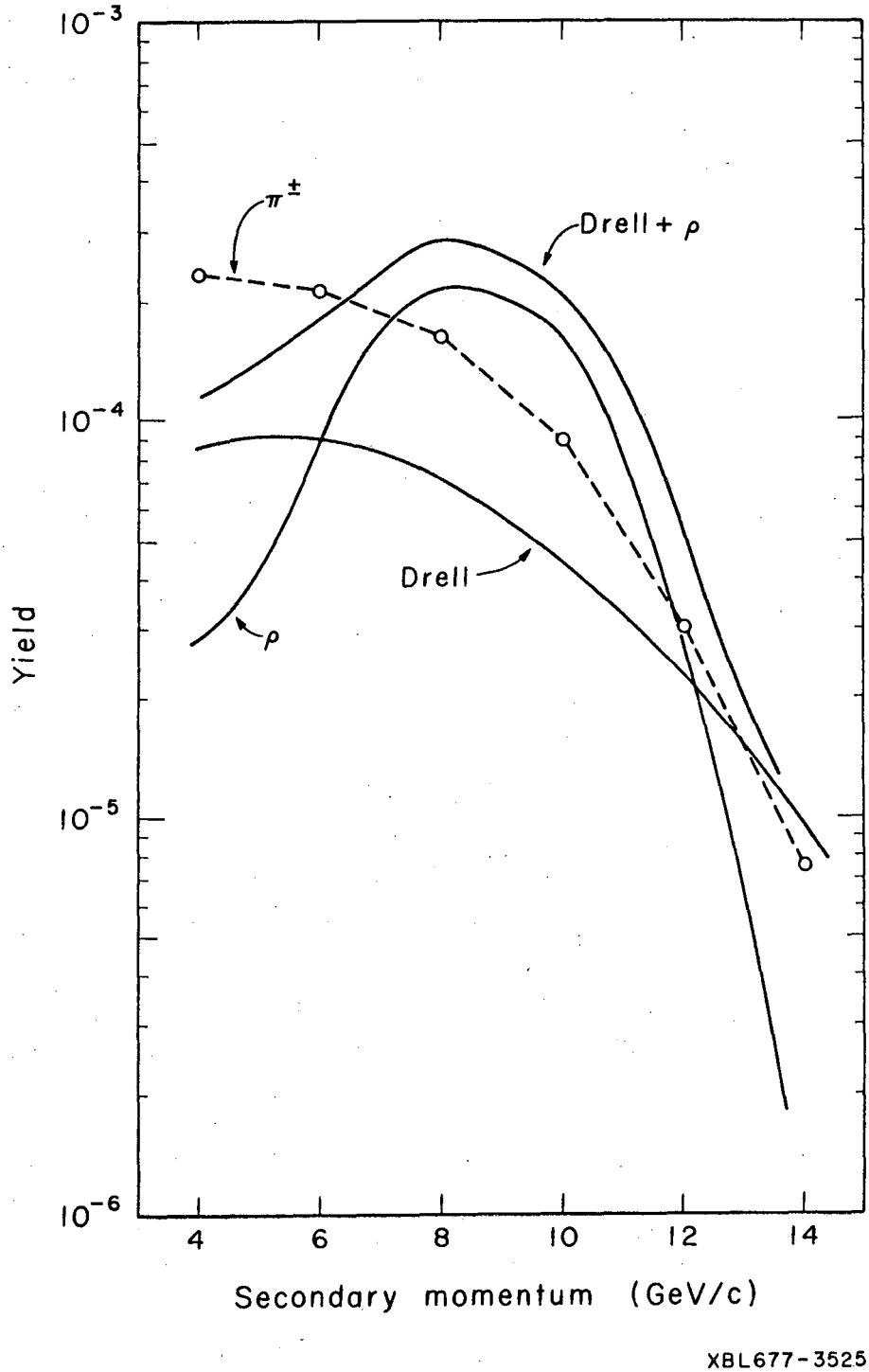
10^{-3}
10^{-4}
10^{-5}
10^{-6}
Yield
$\pi^{\pm}$
Drell + ρ
Drell
ρ
4
6
8
10
12
14
Secondary momentum (GeV/c)
XBL677-3525

Fig. 12

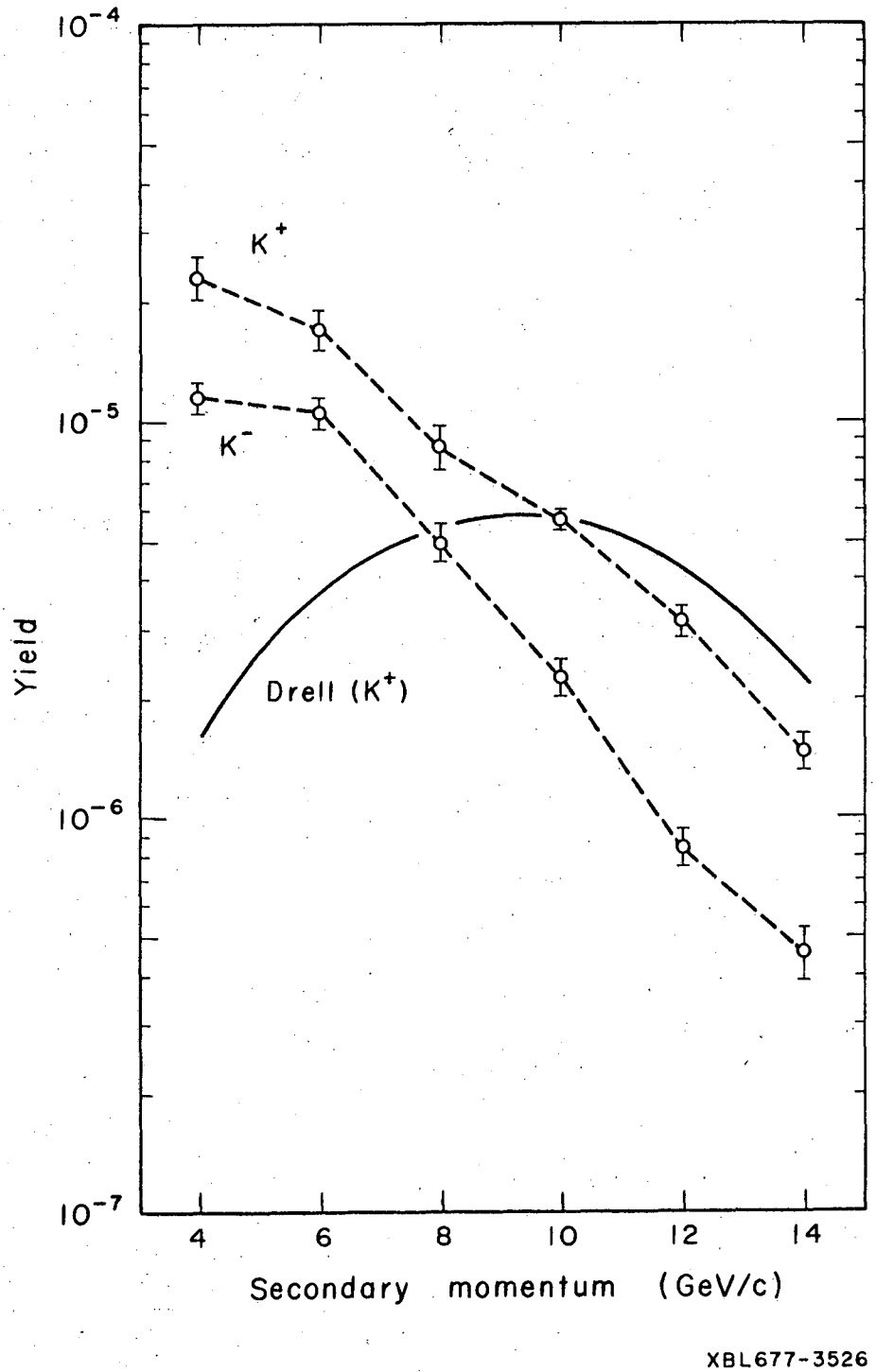
10^{-4}
10^{-5}
10^{-6}
10^{-7}
Yield
K^+
K^-
Drell (K^+)
4
6
8
10
12
14
Secondary momentum (GeV/c)
XBL677-3526

Fig. 13

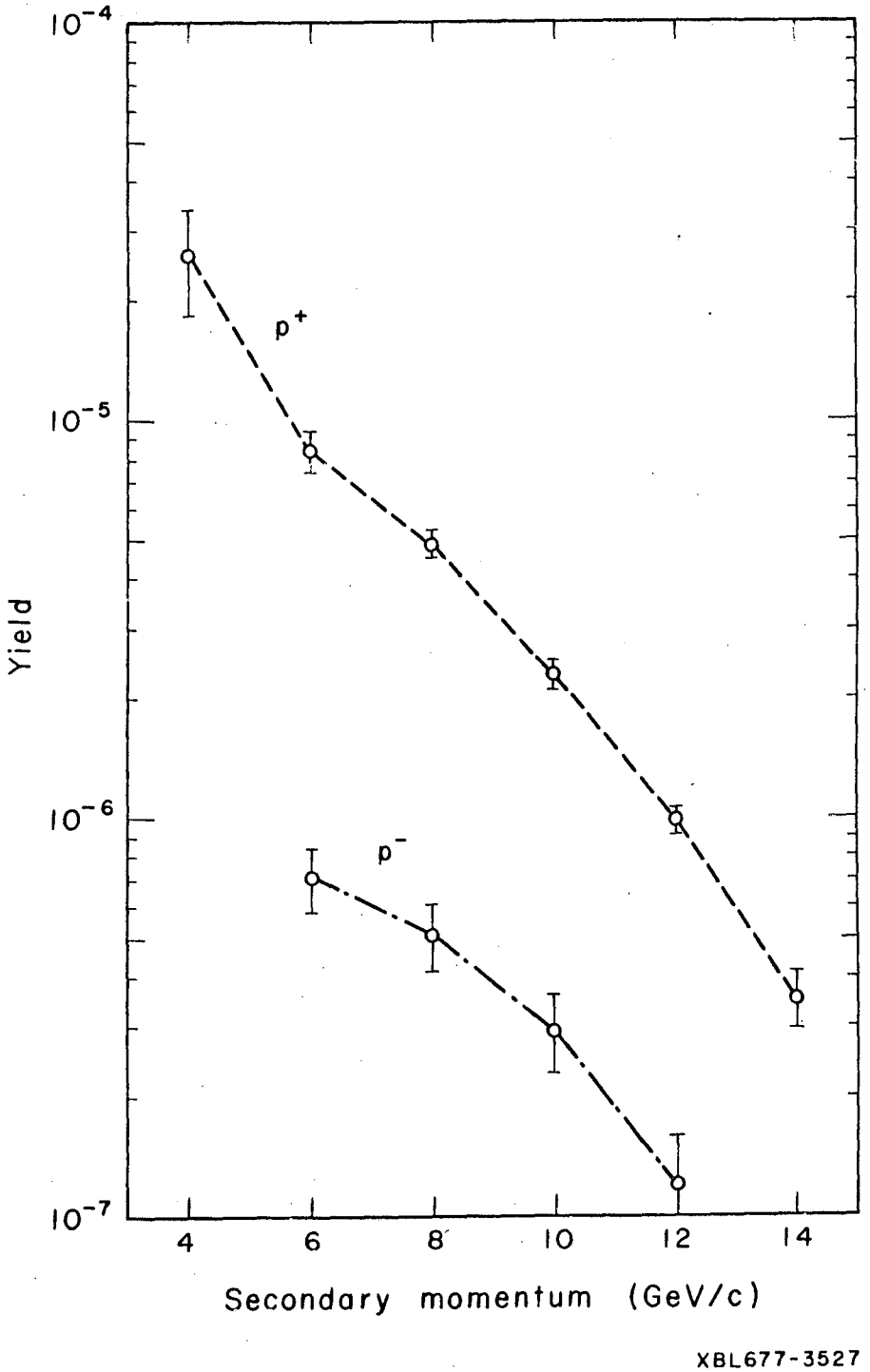
10^{-4}
10^{-5}
10^{-6}
10^{-7}
Yield
p^+
p^-
4
6
8
10
12
14
Secondary momentum (GeV/c)
XBL677-3527

Fig. 14

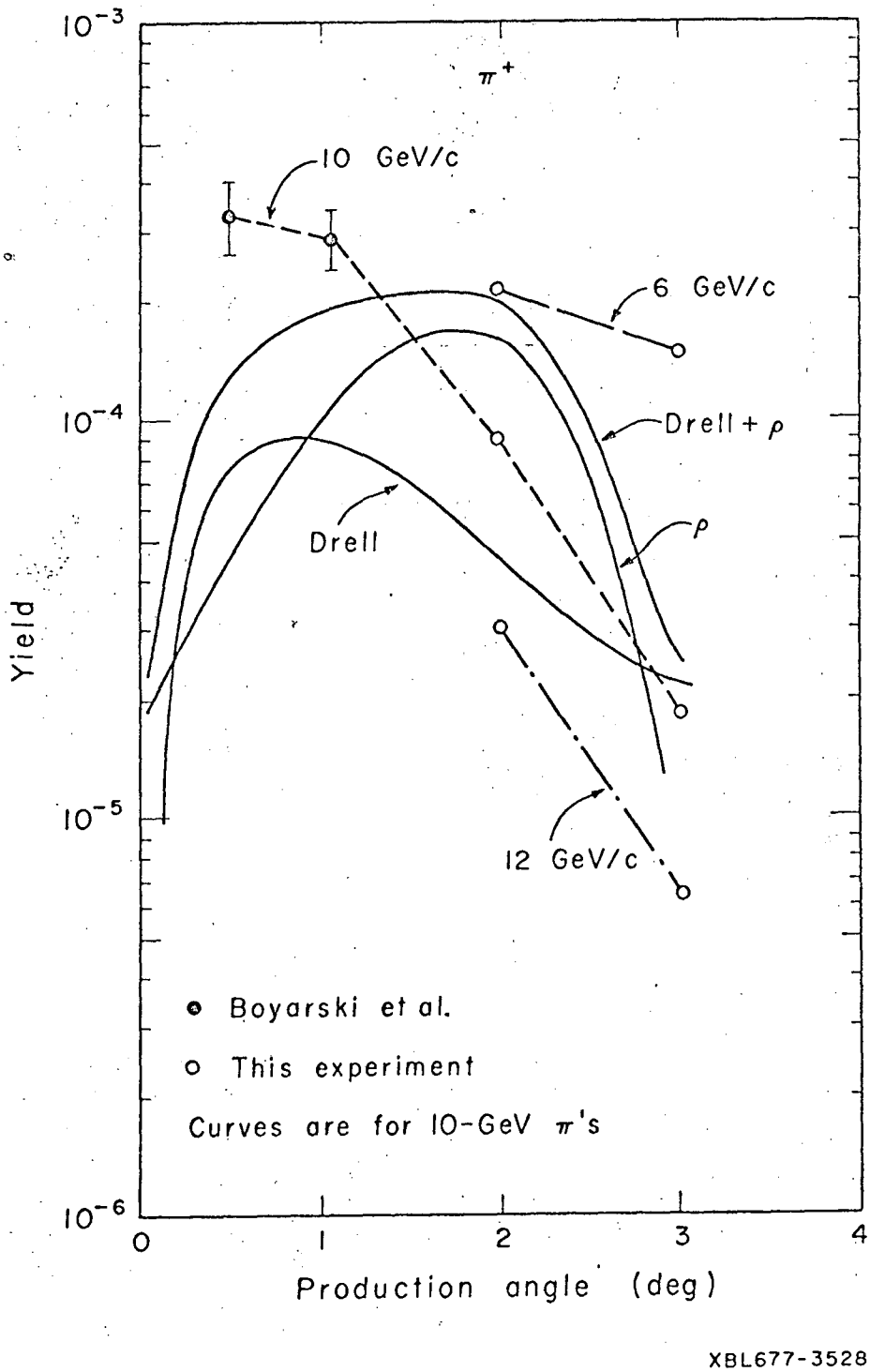
10^{-3}
10^{-4}
10^{-5}
10^{-6}
Yield
π^+
10 GeV/c
6 GeV/c
Drell + ρ
ρ
Drell
12 GeV/c
Boyarski et al.
This experiment
Curves are for 10-GeV π's
0
1
2
3
4
Production angle (deg)
XBL677-3528

Fig. 15

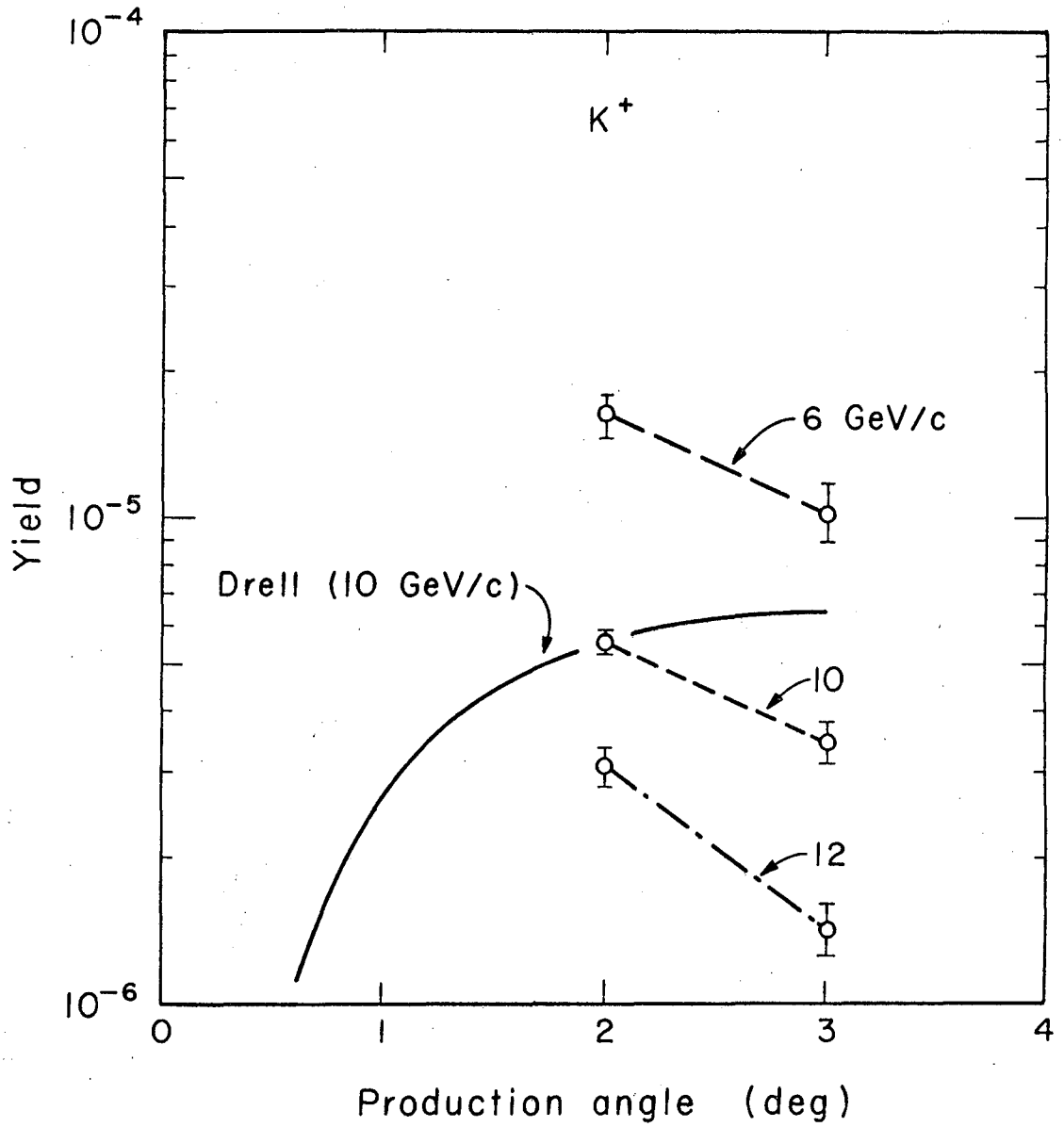
10^{-4}
10^{-5}
10^{-6}
Yield
K^+
6 GeV/c
Drell (10 GeV/c)
10
12
0
1
2
3
4
Production angle (deg)
XBL677-3529

Fig. 16

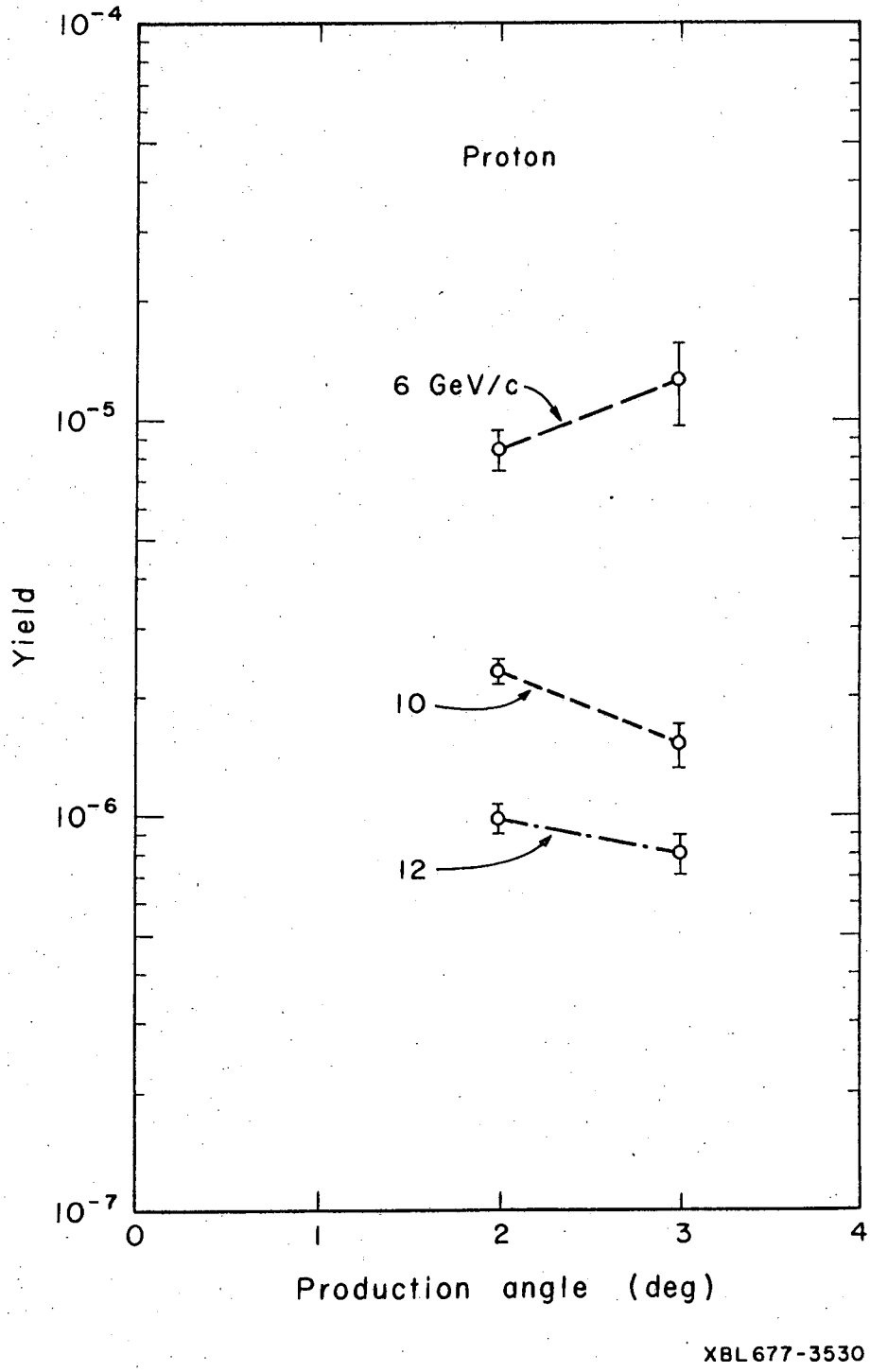
Proton
6 GeV/c
10
12
Yield
10^{-4}
10^{-5}
10^{-6}
10^{-7}
0
1
2
3
4
Production angle (deg)
XBL677-3530

Fig. 17

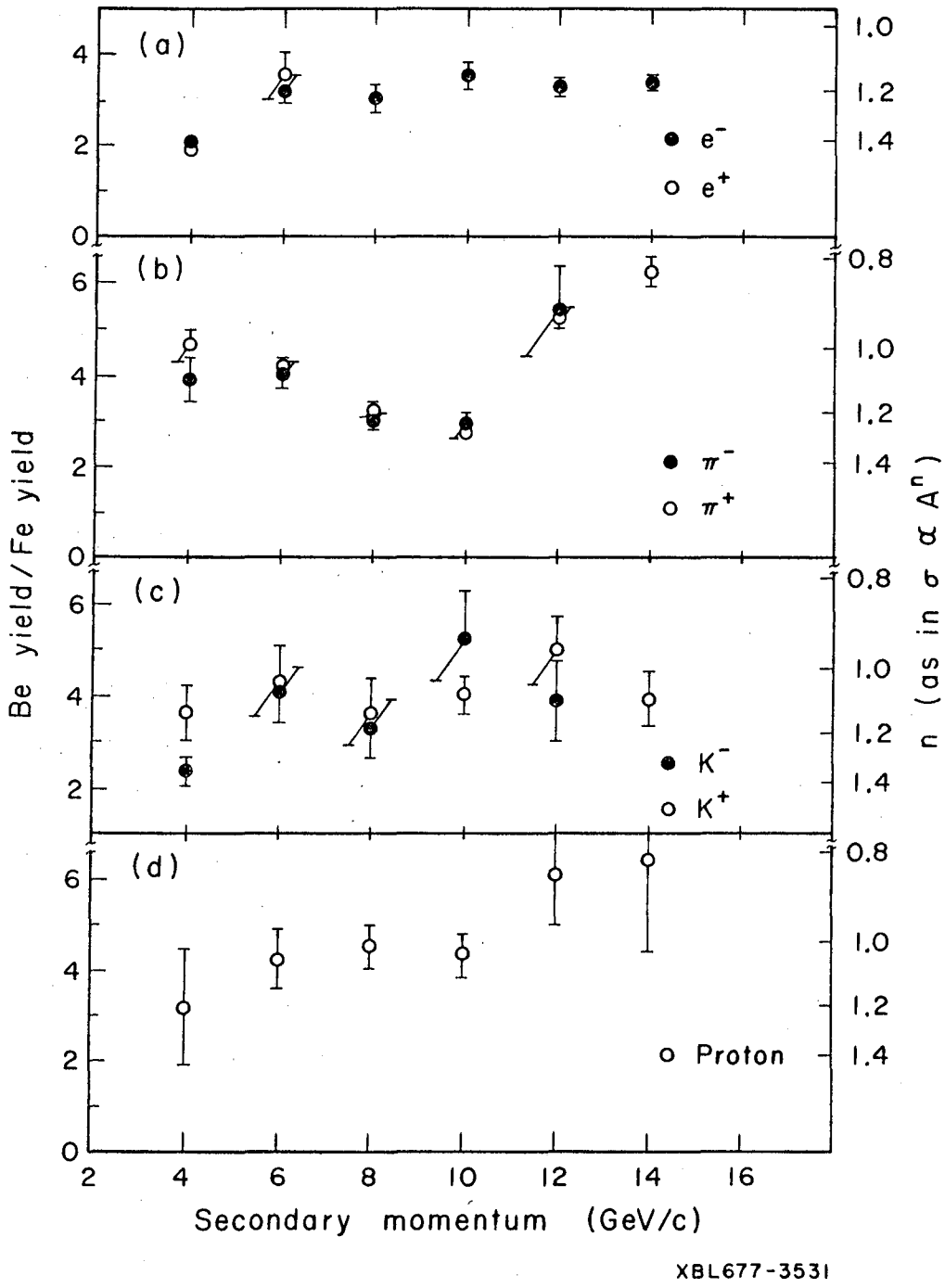
(a)
e⁻
e⁺
(b)
π⁻
π⁺
(c)
K⁻
K⁺
(d)
Proton
Be yield / Fe yield
n (as in σ ∝ Aⁿ)
Secondary momentum (GeV/c)
XBL677-3531

Fig. 18

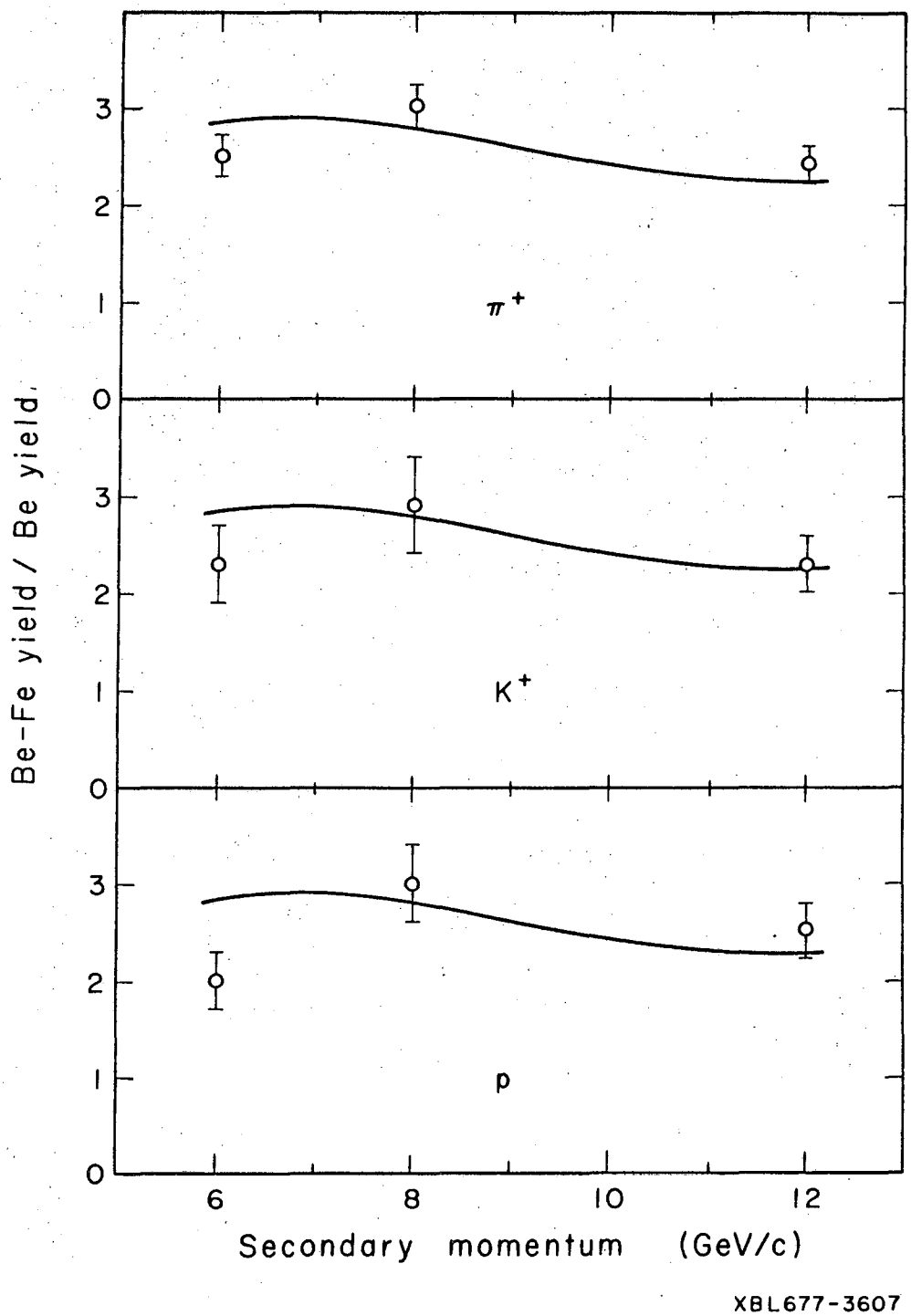
Be-Fe yield / Be yield
3
2
1
0
π^+
K^+
p
6
8
10
12
Secondary momentum (GeV/c)
XBL677-3607

Fig. 19

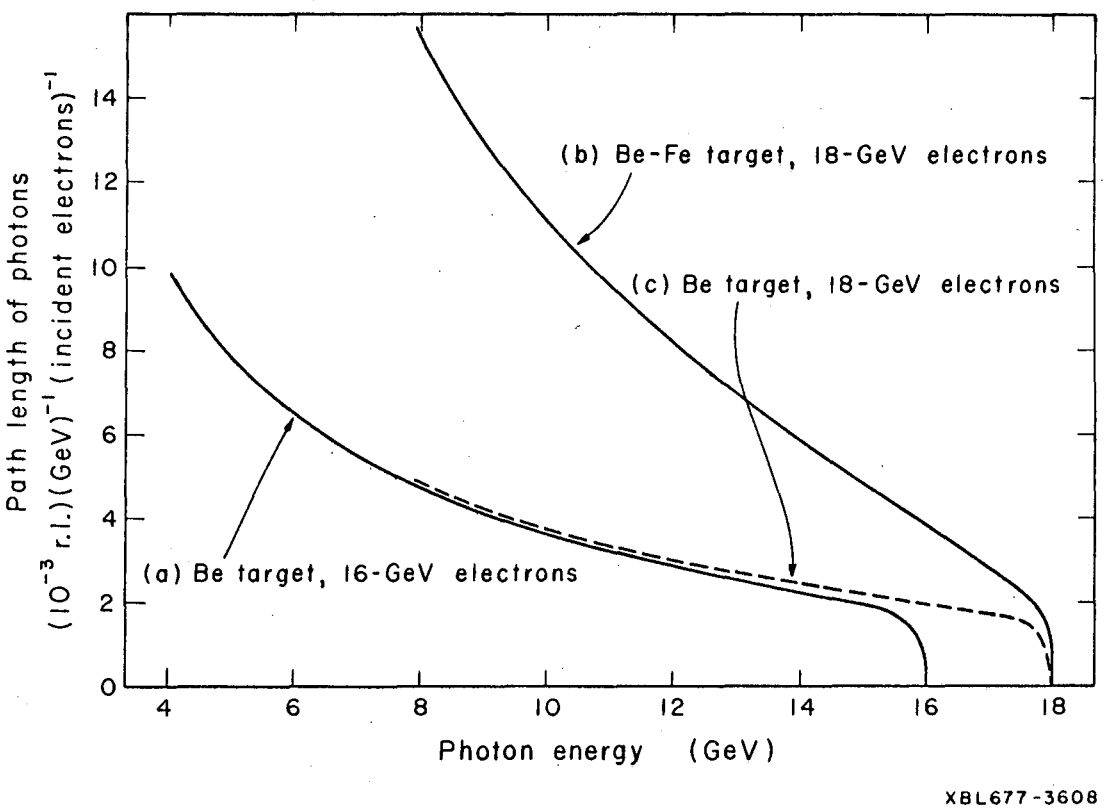
Path length of photons
$(10^{-3}$ r.l.)(GeV)$^{-1}$ (incident electrons)$^{-1}$
0
2
4
6
8
10
12
14
4
6
8
10
12
14
16
18
Photon energy (GeV)
(a) Be target, 16-GeV electrons
(b) Be-Fe target, 18-GeV electrons
(c) Be target, 18-GeV electrons
XBL677-3608

Fig. 20